

UC Irvine

UC Irvine Previously Published Works

Title

Lifetimes and timescales of tropospheric ozone: Global metrics for climate change, human health, and crop/ecosystem research

Permalink

<https://escholarship.org/uc/item/27q8f7ft>

Journal

Elementa: Science of the Anthropocene, 12(1)

ISSN

2785-4558

Authors

Prather, Michael J

Zhu, Xin

Publication Date

2024-02-29

DOI

10.1525/elementa.2023.00112


Copyright Information

This work is made available under the terms of a Creative Commons Attribution License, available at <https://creativecommons.org/licenses/by/4.0/>

Peer reviewed

RESEARCH ARTICLE

Lifetimes and timescales of tropospheric ozone

Michael J. Prather^{1,*}  and Xin Zhu¹

The lifetime of tropospheric O₃ is difficult to quantify because we model O₃ as a secondary pollutant, without direct emissions. For other reactive greenhouse gases like CH₄ and N₂O, we readily model lifetimes and timescales that include chemical feedbacks based on direct emissions. Here, we devise a set of artificial experiments with a chemistry-transport model where O₃ is directly emitted into the atmosphere at a quantified rate. We create 3 primary emission patterns for O₃, mimicking secondary production by surface industrial pollution, that by aviation, and primary injection through stratosphere-troposphere exchange (STE). The perturbation lifetimes for these O₃ sources includes chemical feedbacks and varies from 6 to 27 days depending on source location and season. Previous studies derived lifetimes around 24 days estimated from the mean odd-oxygen loss frequency. The timescales for decay of excess O₃ varies from 10 to 20 days in northern hemisphere summer to 30 to 40 days in northern hemisphere winter. For each season, we identify a single O₃ chemical mode applying to all experiments. Understanding how O₃ sources accumulate (the lifetime) and disperse (decay timescale) provides some insight into how changes in pollution emissions, climate, and stratospheric O₃ depletion over this century will alter tropospheric O₃. This work incidentally found 2 distinct mistakes in how we diagnose tropospheric O₃, but not how we model it. First, the chemical pattern of an O₃ perturbation or decay mode does not resemble our traditional view of the odd-oxygen family of species that includes NO₂. Instead, a positive O₃ perturbation is accompanied by a decrease in NO₂. Second, heretofore we diagnosed the importance of STE flux to tropospheric O₃ with a synthetic “tagged” tracer O3S, which had full stratospheric chemistry and linear tropospheric loss based on odd-oxygen loss rates. These O3S studies predicted that about 40% of tropospheric O₃ was of stratospheric origin, but our lifetime and decay experiments show clearly that STE fluxes add about 8% to tropospheric O₃, providing further evidence that tagged tracers do not work when the tracer is a major species with chemical feedbacks on its loss rates, as shown previously for CH₄.

Keywords: Tropospheric ozone, Air quality, Stratosphere-troposphere exchange, Short-lived climate forcers, Non-linear chemistry, Chemical modes

1. Introduction

Ozone (O₃) is an essential but dangerous component of the atmosphere and the air we breathe. Tropospheric ozone is detrimental to human and plant health and also responsible for about 12% of the greenhouse-gas driven climate change to date (Szopa et al., 2021); yet, it is essential as the primary source of hydroxyl radicals (OH) that cleanse the lower atmosphere of many pollutants (Levy, 1972). The total ozone column, predominantly stratospheric, shields us from ultraviolet-B that damages skin cells (Roffo, 1939; Blum, 1959). The natural chemistry of stratospheric O₃ and its catalytic depletion by a range of anthropogenic trace gases is well recognized (Chapman, 1930; Bates and Nicolet, 1950; Junge, 1962; Danielsen, 1968; Johnston, 1971; Molina and Rowland, 1974; World Meteorological Organization [WMO], 2022). In the

troposphere, O₃ is a secondary pollutant meaning that it is produced chemically from other pollutants (Haagen-Smit, 1952; Haagen-Smit and Fox, 1955; Chameides and Walker, 1973; Fishman and Crutzen, 1978; Logan et al., 1981). Because of this lack of direct emissions, our understanding and modeling of O₃ is quite different from that of other chemical pollutants and greenhouse gases. For example, we do not create atmospheric budgets tied to emissions, and thus we do not derive lifetimes as we do for other gases like methane (CH₄) based on the atmospheric burden divided by emissions. Here, we take a new approach to the study of tropospheric O₃ by simulating a direct emission source of O₃ and then following its perturbation on the background atmosphere to derive that source's lifetime and thence the timescale to remove that excess O₃.

We study the perturbation to O₃ from hypothesized primary emissions associated with (i) surface industrial pollution, (ii) aviation, and (iii) stratosphere-troposphere exchange (STE) using the UC Irvine chemistry-transport model (UCI CTM) with stratospheric-plus-tropospheric

¹ Department of Earth System Science, University of California at Irvine, Irvine, CA, USA

* Corresponding author:
Email: mprather@uci.edu

chemistry. A 3D emission pattern with 100 Tg-O₃ yr⁻¹ is maintained in these experiments. We diagnose the pattern and burden of excess O₃ over different meteorological years. Nominally, we would calculate the “lifetime” of tropospheric O₃ following the standard definition: global O₃ burden (Tg) at steady state divided by total emissions or total losses (Tg yr⁻¹). The budget-based lifetime for a trace gas like methyl bromide (CH₃Br) is based on the burden in all connected reservoirs (i.e., stratosphere, troposphere, ocean mixed layer) (Butler, 1994), but this will not work for tropospheric O₃. The quantity derived here is the “perturbation lifetime” since we ratio the excess burden to the excess emissions. Note that the perturbation lifetime includes the chemical feedbacks, which the global lifetime does not, for example, the CH₄ perturbation lifetime is about 1.4 times larger than the global lifetime because of methane’s feedback on its chemical loss rate (Isaksen and Hov, 1987).

We follow the decay of the excess O₃ after emissions are cut and calculate a timescale for the O₃ perturbation from the long-term e-fold rate. The timescale is nominally that of the longest-lived chemical mode involving tropospheric O₃, which is an inherent property of the atmosphere; whereas the lifetime depends on the location of emissions because the emissions are exposed to different photochemical activity. This relationship between lifetimes and timescales is well-known for CH₄ (Isaksen and Hov, 1987; Prather, 1994, 1996), CH₃Br (Butler, 1994; Prather, 1997), and other gases (Prather, 2007), but has not yet been explored for tropospheric O₃. Because chemical feedbacks are included in both the temporal decay and the perturbation lifetime, both values are expected to be similar.

The experimental design, O₃ chemistry, and specific experiments are presented in Section 2. The steady-state lifetime and patterns are analyzed in Section 3. Section 4 discusses the implications of this work including: lifetimes, tagged tracers, perturbations to other species, and the odd oxygen family. The results here are inconsistent with some conclusions about the stratospheric influence on tropospheric O₃ using tagged tracers like O3S (Follows and Austin, 1992) and, further, question the use of odd-oxygen (Bates and Jacob, 2019) as a way to understand tropospheric O₃.

2. Methods

2.1. Defining production and loss of tropospheric O₃

In current chemistry-climate or chemistry-transport models (CCMs or CTMs), the chemical continuity equation for O₃ is usually calculated correctly using all the rates directly involving O₃. The local, grid-cell equation for O₃ chemical tendency looks like

$$\begin{aligned} d[\text{O}_3]/dt = & + k(T, M) [\text{O}] [\text{O}_2] - J(\text{O}_3) [\text{O}_3] \\ & - k(T) [\text{O}_3] [\text{NO}] - k(T) [\text{O}_3] [\text{HO}_2] - \dots \end{aligned} \quad (1)$$

where all chemical reactions directly involving [O₃] are included. Because of the rapid exchange of O and O₃, the first 3 terms largely cancel one another; and the timescales of the system are not represented by the negative loss terms divided by [O₃]. For example, the photolysis

frequency $J(\text{O}_3)$ does not represent any of the timescales of the O₃-O system as shown in the eigenvalue decomposition of Chapman O₃ chemistry (Section 3 of Prather, 2007). The desire to remove these large rates from the O₃ chemical budget, in part to estimate a more realistic loss rate and timescale, has led to complex definitions of the family grouping called odd oxygen,

$$\text{O}_X \equiv \text{O}_3 + \text{O} + \text{NO}_2 + 2 x \text{NO}_3 + \dots \quad (2)$$

Because O₃ is the dominant species in the O_X family, the loss of O_X is expected to represent the lifetime and timescales of O₃ in the stratosphere or troposphere (Nicolet, 1975; Thrush, 1980; Bates and Jacob, 2019; Badia et al., 2021). The problem is that these family groupings, while intuitive and comforting, do not accurately produce the correct timescales or patterns of perturbations to the chemical system. We show later that the O_X family is not one of the inherent chemical mode patterns of the troposphere and has the wrong timescales.

The tropospheric chemistry community has for the most part settled on diagnosing production and loss of tropospheric O₃ in the global models from the major rates for the O_X budget, for example, from Table 4.12 in the 2001 IPCC assessment (Prather et al., 2001) to Table 6.3 in the 2021 assessment (Szopa et al., 2021).

$$\begin{aligned} \text{PO}_X = & k_1(T) [\text{HO}_2] [\text{NO}] \\ & + k_2(T) [\text{RO}_2] [\text{NO}] \text{ (sometimes } + 2 x J_{\text{O}_2}[\text{O}_2]) \end{aligned} \quad (3)$$

$$\begin{aligned} \text{LO}_X = & k_3(T) [\text{O}({}^1D)] [\text{H}_2\text{O}] + k_4(T) [\text{O}_3] [\text{HO}_2] \\ & + k_5[\text{O}_3] [\text{OH}] \end{aligned} \quad (4)$$

For the global troposphere, the history of major model intercomparison projects (MIPs) have reported PO_X and LO_X in the range of 3500–5000 Tg-O₃ yr⁻¹ with the balance of the budget made up of a source from STE (400–600 Tg-O₃ yr⁻¹) and a sink to surface deposition (800–1200 Tg-O₃ yr⁻¹) (Prather et al., 2001; Stevenson et al., 2013; Young et al., 2018; Archibald et al., 2020; Griffiths et al., 2021; Szopa et al., 2021). These diagnostics reflect the major rates affecting O₃; they are now standard diagnostics for current chemistry models; and they have served as excellent diagnostics for understanding consistency and differences in the model calculated O₃.

The extensive use of PO_X and LO_X has created 2 problems. First, everyone has known that the true O₃ chemical tendency ($d\text{O}_3/dt$, Equation 1) is not exactly equal to PO_X–LO_X. Recently, the Archibald et al. (2020) study of tropospheric O₃ trends made a substantial effort to include the $d\text{O}_3/dt$ budget term in analyzing the 4 models that reported it, finding that it provided “a cleaner . . . account of the tendency of ozone” due to chemical processes. Hopefully, this effort will continue in future MIPs.

The second major problem with the O_X terms is the assumption that the O₃ chemical tendency equation can be written as at

$$d[\text{O}_3]/dt = +\text{PO}_X - f\text{O}_{3\text{chem}}[\text{O}_3] \quad (5)$$

where the production PO_X is constant, independent of $[O_3]$, and the loss frequency is calculated simply from LO_X ,

$$fO_{3\text{chem}}^{LO_X} = LO_X / [O_3] \quad (6)$$

This approach is popular and persistent because it puts O_3 in a parallel framework with other trace gases where production is due to sources that are independent of the species concentration and where loss is linearly proportional to the species concentration.

Follows and Austin (1992) with a 2D model and Røefols and Lelieveld (1997) with a 3D model developed the approach of using the tagged tracer O3S in order to follow stratospheric O_3 entering the troposphere through STE. Using their photochemical box model, Follows and Austin (their Figure 10) followed the decay of an O_3 perturbation using full chemistry as is done here with a 3D model, but they reverted to using the simplified and inaccurate linear assumptions about LO_X (their Equation 11). This methodology continues in multimodel assessments of O_3 and climate change, such as Williams et al. (2019) and Abalos et al. (2020). Wild et al. (2003) used this O3S method but recognized that “this [approach] is not a correct linearization of the impact of an added flux of stratospheric ozone,” yet we have all continued using this approach for the last 2 decades. The loss frequency for O_3 should be derived from a linearization of the chemical tendency

$$fO_{3\text{chem}}^{\text{TRUE}} = d[-dO_3/dt] / d[O_3] \quad (7)$$

but 3D models are not prepared to do chemical linearizations every time step. Using the ATom-1 observations, Prather et al. (2023, Figure 68) showed that LO_X is not precisely linear in $[O_3]$, and more importantly that PO_X is not constant but decreases with increasing $[O_3]$. Hence, $fO_{3\text{chem}}^{\text{TRUE}}$ is 20%–40% larger than $fO_{3\text{chem}}^{LO_X}$, and thus currently modeled O3S values are too large. From the limited coverage of ATom observations we cannot derive a global pattern of $fO_{3\text{chem}}^{\text{TRUE}}$, but here we can calculate hemispheric mean values from the decay of O_3 perturbations.

2.2. The control run

The baseline for this study is a UCI CTM 5-year control run (CTRL) for years 2000 through 2004 that includes stratospheric-plus-tropospheric gas-phase chemistry with typical emissions and boundary conditions for years 2000 through 2004 (see Tang and Prather, 2012; Holmes et al., 2013; Holmes et al., 2014). The CTM is driven by prescribed meteorology from the European Centre for Medium-Range Weather Forecasts Integrated Forecast System (Cycle 38r1). Use of historical, specified meteorological fields for January 1, 2000 through December 31, 2004 means that any chemical perturbation can be tracked accurately to within the relative precision of the nonlinear chemical solver, about 10^{-5} . With a CCM, these experiments would require a number of ensembles to average the perturbations over climate variability, but here a single perturbation and control simulation are adequate. A summary of the UCI CTM chemistry and conditions for the CTRL run are given in the Appendix Tables A1–A3. A

summary of the tropospheric O_3 budget (Table 1) has the UCI CTM falling within the range of models tabulated in recent MIPs (Young et al., 2018; Archibald et al., 2020; Griffiths et al., 2021).

For this study it is essential to be able to separate the troposphere from stratosphere, and thus we use instantaneous 3D fields of O_3 and e90, our artificial tracer of tropospheric air (Prather et al., 2011). The e90 tracer has a constant rate of decay (90 days) and is emitted uniformly over the globe at a rate to generate an average abundance of 100 ppb (nmol/mol). In this version q75 of our CTM, e90 = 90 ppb coincides with the WMO tropopause and is used to categorize each grid cell as either tropospheric or stratospheric. Monthly averages of O_3 and e90, or even WMO tropopauses, smear across the synoptic variability of the tropopause, causing systematic errors in diagnosing tropospheric O_3 . We compromise on continuity versus data volume by using 73 snapshots per year (every 5 days) that record the 3D mass fields of O_3 , e90, and dry air in each cell. The zonal-mean altitude-by-latitude color maps of CTRL stratospheric and tropospheric O_3 are shown in Figure 1 and Figures A1–A2. Results here average over 18 snapshots in the 90 days of northern summer (JJA) over the 5 years and are typical of other models and observations. The seasonal and zonal average for stratospheric O_3 includes only stratospheric cells, so that if at least one of the 320 longitude cells over the 18 snapshots is stratospheric a non-blank value is shown for that pixel. Thus, the same pixel can be included in both figures.

The annual variability in global mean stratospheric and tropospheric O_3 in Dobson units (DU) is shown in Figure 2 and Figure A3. Over the 5-year CTRL run, the tropospheric mean column varies from about 28 DU (Feb) to a sharp peak of about 34 DU (Oct) occurring within a 10-day period (1 DU global = 10.9 Tg- O_3). These values are consistent with the observed columns (about 30 DU) and seasonal cycle (minimum in DJF) found by Ziemke et al. (2006, 2012). This synoptic 5-day variability as well as the interannual changes are driven by the meteorological changes (H_2O , T, transport) since emissions vary only monthly and are recycled each year. Likewise, the lower boundary conditions for CH_4 , H_2 , and N_2O are constant. Lightning NO emissions are tied to convection but vary at most by 6% from year to year. In contrast, the stratospheric column varies smoothly, from 270 DU (approximately Sep–Oct) to about 290 DU (Mar). This stratospheric O_3 annual cycle along with the longer-term quasi-biennial variability matches latitudinal patterns seen in satellite observations (Figure 9 of Ruiz and Prather, 2022). Looking at the synoptic variability, one might infer that the sharp tropospheric O_3 peak in Oct is carried into the stratospheric O_3 column and thus long-term tropospheric O_3 trends and variability will alter the stratospheric O_3 column.

2.3. Simulating direct O_3 emissions

Trying to diagnose the budget lifetime and timescales of tropospheric O_3 perturbations from a combination of reaction rates or their derivatives with respect to O_3 is

Table 1. CTM experiments

Run	Emissions					Notes		
CTRL	Control run							
eO3avi (EO3A)	+100 Tg-O ₃ yr ⁻¹					Aviation: NO emission pattern, RCP6.0 y2000		
eNOavi (EO3B)	+0.85 Tg-N yr ⁻¹ (2×Aviation NO _x)					Aviation: NO emission pattern, RCP6.0 y2000		
eO3srf (EO3S)	+100 Tg-O ₃ yr ⁻¹					Surface: 34°N–40°N; 110°E–140°E; 0–2 km		
eO3ste1 (EO3T)	+100 Tg-O ₃ yr ⁻¹					STE: 25°S–35°S & 27°N–37°N; 11.0–12.2 km		
eO3ste2 (EO3U)	+100 Tg-O ₃ yr ⁻¹					STE: 15°S–25°S & 15°N–25°N; 11.0–12.2 km		
CTRL: O ₃ Budget	P–O ₃	L–O ₃	P–L (O ₃)	DD–O ₃	Residual (STE)	L–O _x	Mean Loss Frequency	
Tg-O ₃ yr ⁻¹	23,963	23,695	269	628	359	4,656	(23.8 days) ⁻¹	
Perturbation O ₃ Burden (Tg-O ₃)					Perturbation O ₃ Lifetime (Days)			
Run	Troposphere		Stratosphere		Troposphere			
CTRL	345		3,045		Na			
eO3avi	5.32 (4.28–6.98)		1.66 (0.63–2.70)		19 (16–25)			
eNOavi	4.82 (4.14–5.24)		0.34 (0.22–0.45)		Not defined			
eO3srf	3.46 (1.59–5.77)		0.16 (0.10–0.25)		13 (6–21)			
eO3ste1	6.84 (6.35–7.49)		3.59 (2.51–4.73)		25 (23–27)			
eO3ste2	6.44 (6.09–7.00)		0.98 (0.69–1.39)		24 (22–26)			

Notes: All UCI CTM results are averaged over 3 years (2001–2003). The O₃ budget for CTRL is similar to other models for present day (1995–2004) in Table 1 of Griffiths et al. (2021) and Figure 3 of Young et al. (2018). Note that P (L) of O₃ are derived from the positive (negative) terms in Equation 1, so that P–L is the true $d[\text{O}_3]/dt|_{\text{chem}}$ of Archibald et al. (2020). L–O_x is taken from Equation 4 and can be directly compared with “L” in these MIP tables. The mean loss frequency is calculated as the burden (345 Tg) divided by the sum of dry deposition (628 Tg yr⁻¹) plus L–O_x (4,656 Tg yr⁻¹). Burden (Tg-O₃) and lifetime (days) for the eO3xxx experiments are shown as: mean (min–max). Perturbation lifetime assumes that effectively all emissions (100 Tg-O₃yr⁻¹) are going into the troposphere, even if some originates in the stratosphere. Shorthand notation for files and some legends is shown in “EO3X” format. CTRL = control; MIP = model intercomparison project; STE = stratosphere–troposphere exchange; UCI CTM = UC Irvine chemistry-transport model.

an unrewarding task. So instead we propose a CTM model experiment in which we directly emit O₃ at a fixed rate (100 Tg-O₃ yr⁻¹) for several years and follow the increased burden of O₃. This perturbation allows all of tropospheric chemistry to change in response and gives us the perturbation lifetime for that specific pattern of emissions. Then, we cut emissions and watch the decay time of the chemical modes so we can diagnose the timescale of O₃ perturbations. Remembering the eigenvalue decomposition of the system (Prather, 2007), we expect the lifetime (i.e., burden in this case) to depend on the location-timing of emissions, but the timescale of each chemical mode will be a property of the CTRL atmosphere and independent of the emission pattern. The amplitude of each mode, however, will depend on the emission pattern.

The direct O₃ emissions are added as a perturbation to a CTRL run simulation and are designated eO3x, where “x” designates the specific case, see **Table 1**. Three different types of direct O₃ emissions are explored: eO3avi, 100 Tg-O₃ emitted per year using the same pattern as aviation NO_x; eO3srf, 100 Tg-O₃ yr⁻¹ as near-surface emissions from east Asia (34°N–40°N; 110°E–140°E), consistent

with the net production of 130 Gg per day found for East Asia (Wild and Prather, 2006); and eO3ste1, 100 Tg-O₃ yr⁻¹ centered on the subtropical jets, meant to simulate a fraction of the net influx of stratospheric O₃ (as modeled in Prather et al., 2011; Ruiz and Prather, 2022). The first eO3ste1 experiment resulted in large amounts of O₃ accumulating in the stratosphere, which complicated the calculation of O₃ lifetime. Thus, we relocated the emissions and reran this experiment as eO3ste2, see the latitude shift of emissions in **Table 1**. To compare the O₃ perturbation from direct emissions versus the secondary O₃ produced from aviation NO_x, we added experiment eNOavi, for which the aviation NO_x emissions (0.85 Tg-N yr⁻¹) are doubled. See **Table 1** for details of each experiment.

The eO3x experiments are run for 4 years (2000.0 to 2004.0). For eO3avi, eO3srf, and eO3ste1, we run separate 6-month decay experiments, cutting the direct O₃ emissions at 2003.5 (1 Jul) and 2004.0 (1 Jan). **Figure 2** shows the resulting perturbations in DU for eO3avi tropospheric (blue) and stratospheric (red) O₃. Figure A4 shows parallel results for eO3srf and eO3ste1. Our estimated lifetime for the eO3avi O₃ perturbation, 20 days, is similar to most

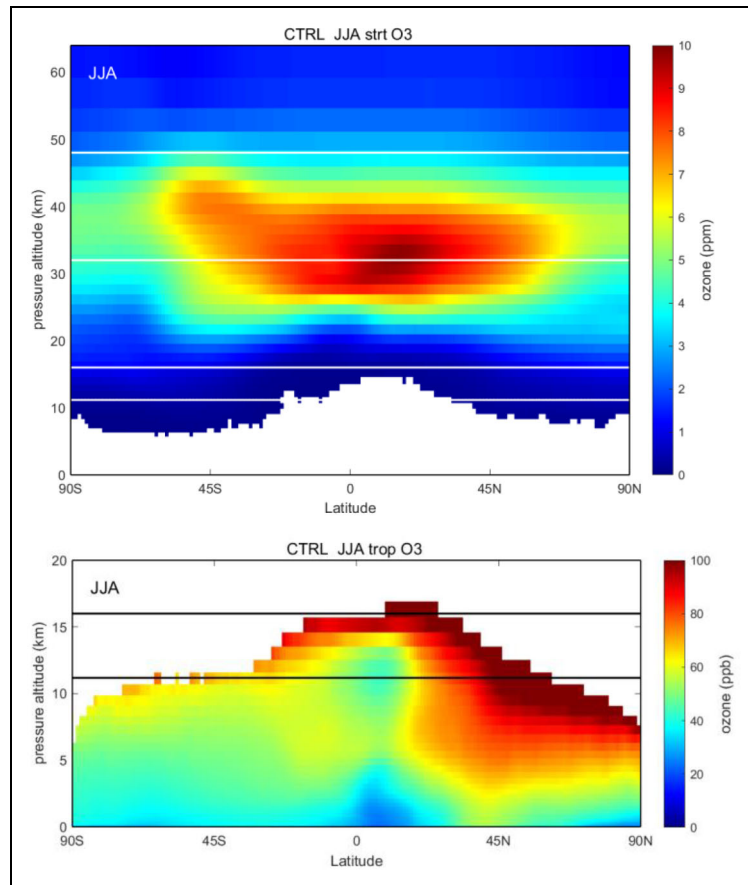


Figure 1. Stratospheric and tropospheric zonal mean O_3 abundance (ppm and ppb, respectively) averaged over June–July–August using 18 5-day snapshots from the CTRL run. Coordinates are latitude by pressure altitude $z^* = 16 \text{ km} \log_{10}(1/P(\text{bars}))$ and assume a surface pressure everywhere of 1 bar. Some pixels in this plot contain both stratospheric and tropospheric values because the pixel contained was both stratospheric and tropospheric air over the 18 snapshots and 320 longitude cells (e.g., stratospheric intrusions).

previous values for total tropospheric lifetime (e.g., Badia et al., 2021). Thus, the O_3 lifetime is subseasonal, <1 month; and O_3 perturbations will not mix between hemispheres and will respond to the seasonal variations in photochemical activity. With a fixed boundary condition on CH_4 , the longest chemical response will likely be CO (approximately 2 months) and thus the spin-up and decay times as seen are at most 6 months. Statistics on the O_3 perturbations (**Table 1**) use only the 2nd through 4th year.

Several experiments (eO3avi, eO3ste1, eO3ste2) result in a minor fraction of O_3 emissions occurring in the stratosphere. We tried to minimize direct stratospheric emissions but did not rewrite the CTM code to turn on/off emissions at every time step for each grid cell based on the e90 tropopause definition. In our studies, these direct stratospheric emissions occur well below 100 hPa and thus accumulate mainly in the lowermost extratropical stratosphere (LMS). Ozone chemistry in the LMS, except for the Antarctic ozone hole, is slow, and transport into the troposphere occurs mostly within a year. Thus, direct O_3 emissions into the LMS tend to accumulate until they are transported into the troposphere via STE, and thus the $100 \text{ Tg-O}_3 \text{ yr}^{-1}$ emissions in eO3avi, eO3ste1, and eO3ste2 can be treated tropospheric emissions albeit with some seasonal delay from the STE flux.

3. Results

The lifetimes and patterns of the O_3 perturbations are distinct to each type of emission. The perturbations are all responding to tropospheric chemistry that is damping the perturbations at different locations and seasons according to the photochemical reactivity. For a quick survey of the profiles and variability of production and loss of O_x over the Pacific basin from a multimodel comparison, see Figure 3bc of Prather et al. (2017) and from the NASA Atmospheric Tomography Mission (ATom) observations, see Figures 6–7 of Prather et al. (2023). From the observations, there is large high-frequency variability on the scale of a model grid; and from the models, there are large differences in mean profiles.

3.1. Spatial pattern of O_3 perturbations

The zonal mean (latitude by altitude) pattern of O_3 absolute perturbations (ppb) are shown in **Figure 3** for JJA, showing eO3avi (left) and eO3srf (right) separated by stratosphere (top) and troposphere (bottom). Parallel plots are shown for all 4 seasons and all 5 experiments in Figures A5–A9. For these plots, the stratospheric and tropospheric color bars are same (0 to 12 ppb); plotting relative differences would greatly reduce the intensity of the stratospheric perturbation.

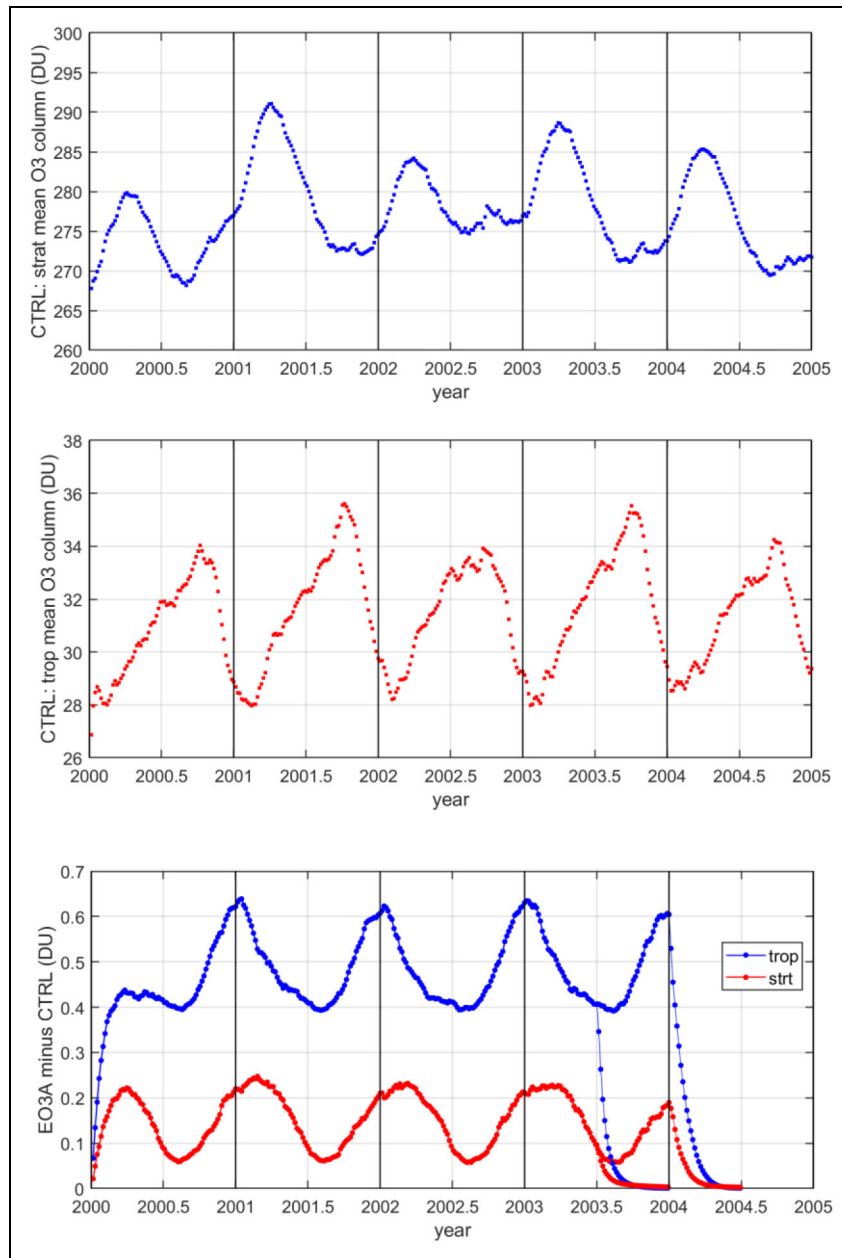


Figure 2. (top panels) Stratospheric and tropospheric mean O₃ columns (DU) from the CTRL run calculated from the 365 5-day snapshots over the 5 years, 2000 through 2004. (bottom panel) Perturbation in the O₃ column (DU) for eO₃avi (EO3A), separating troposphere (blue) from stratosphere (red). Also shown are the decay of the eO₃avi perturbations after cessation of emissions on July 1 (2003.5) and Jan 1 (2004.0). In terms of global column, 1 DU = 10.9 Tg-O₃, and thus 100 Tg-O₃ yr⁻¹ = 9.2 DU yr⁻¹, and a tropospheric column perturbation of 0.5 DU corresponds to a lifetime of 20 days.

Aviation emissions, eO₃avi, include a number of high-latitude, stratospheric flight routes below 12 km altitude (lowest horizontal black line in **Figure 3**). These emissions are seen clearly by the build-up of a 10–12 ppb perturbation from 8 to 12 km in the stratosphere. There is some transport of excess O₃ to higher altitudes in the tropics along isentropic surfaces, but this does not get above 16 km altitude and stays in the LMS. Chemical loss of the excess O₃ is more rapid in the troposphere as is vertical mixing, and the peak build-up in northern mid-latitude flight lanes (8–12 km) is less, about 6 ppb. In northern summer, the loss of excess O₃ is rapid in the

lower troposphere, and the excess O₃ barely reaches the surface with perturbations of approximately 1 ppb. In northern winter (DJF, **Figure A5**) with much slower chemistry, surface perturbations are much greater, approximately 3 ppb. Emissions in the southern midlatitudes are much smaller and barely show up in the stratosphere (approximately 1 ppb) and not in the troposphere with this color scale.

For surface emissions (eO₃srf), the peak zonal mean perturbations are 4–6 ppb in the latitude-altitude region of emissions (black box in **Figure 3**). These emissions are mixed upward to the tropopause at levels of

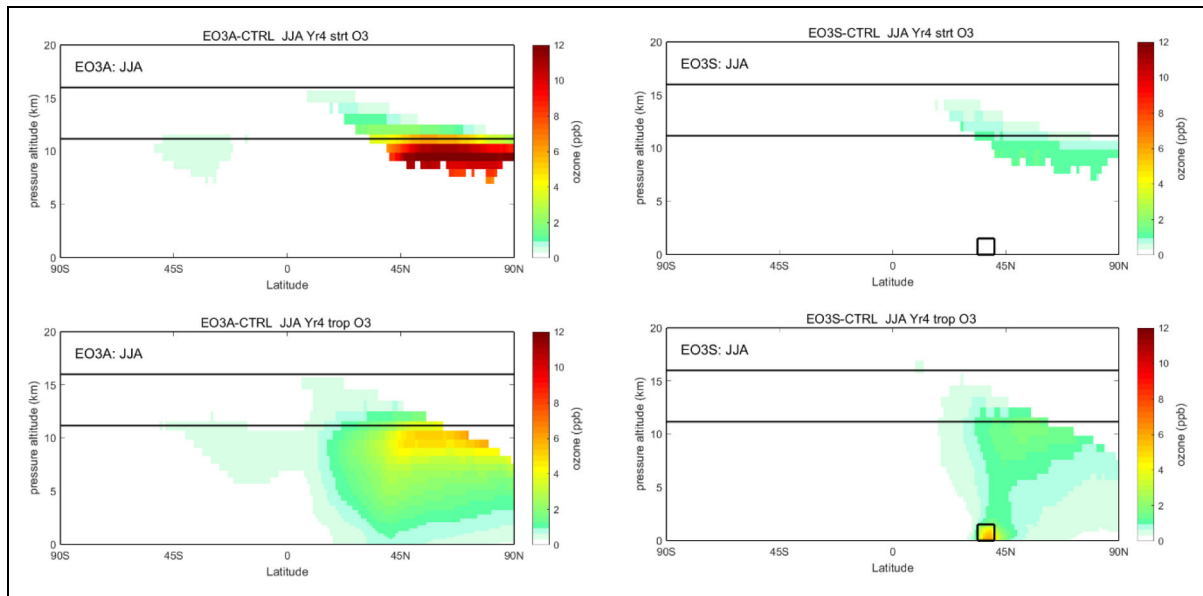


Figure 3. Perturbation to zonal mean O_3 abundance (ppb) in boreal summer (JJA) for eO3avi (EO3A, left panels) and eO3srf (EO3S, right panels) split into stratospheric (top panels) and tropospheric (bottom panels). For methodology, see Figure 1. Aviation emissions eO3avi occur mostly in the northern troposphere but reach into the stratosphere and southern hemisphere. Surface emissions eO3srf occur within the black square over a limited longitude range, see Table 1. Note that color bars have the same range on all plots.

approximately 2 ppb but fall off rapidly in the subtropics and at higher latitudes, again because of the rapid loss of excess O_3 in the northern summer lower troposphere. It is interesting that summertime O_3 pollution from the northern midlatitudes is not expected to reach the polar lower troposphere, but during the other 3 seasons (September–November, December–February, March–May) the surface emissions in eO3srf collect at moderately high levels (approximately 3 ppb) throughout the midlatitude and polar troposphere (Figure A7). eO3srf has no direct stratospheric emissions, and so the LMS enhancement of approximately 2 ppb is driven by the tropospheric increases.

The O_3 perturbations patterns for eO3ste1 and eO3ste2 (Figures A8–A9) are quite different in the stratosphere because of eO3ste1's much greater fraction of emissions directly into the stratosphere; however, their tropospheric patterns are quite similar because the net tropospheric emissions are almost identical as explained above. Focusing on the latitude-altitude patterns for eO3ste2 (Figure A9), it appears to be difficult in any season for the STE O_3 flux to reach the surface in midlatitudes. The simplest explanation is that this flux mostly enters the troposphere about the tropical jet stream and is transported first along isentropic surfaces into the subtropics where chemical loss of O_3 remains high year-round.

3.2. Variability in O_3 columns

The O_3 column (DU) in these experiments is split into stratosphere and troposphere using the 5-day snapshots. The latitude-by-day plot of these 2 columns for CTRL year 2003 (Figure A10) shows the variability of this high-frequency sampling: the Antarctic ozone hole is clear as are the Arctic wintertime vortex breakdowns (Feb–Apr),

which bring high O_3 columns (>450 DU) to the pole. In our experiments, most of the perturbations to column O_3 are dominated by the troposphere except for eO3ste1. Zonal mean O_3 column perturbations versus latitude are shown for all 5 experiments in Figures A11–A15 from years 2000 through 2003. The spin up of the perturbation in the first half of year 2000 is notable in all experiments. The STE experiments eO3ste1 and eO3ste2 show minimal seasonal variability and clear hemispheric symmetry. The southern hemisphere (SH) has a slightly larger build-up, probably because the northern hemisphere has greater pollution and more rapid O_3 loss. The surface emissions eO3srf shows a clear peak column perturbation of approximately 2 DU over the source region near $38^\circ N$, with equally large wintertime maxima extending to $90^\circ N$. The direct aviation emissions eO3avi shows a similar pattern to eO3srf but with less variability since the source is more diffuse. Aviation NO_x emissions eNOavi have a distinct seasonality because of the photochemical variability in the production of O_3 from the NO_x perturbation. eNOavi peaks in the summer and fall (as opposed to winter in eO3avi) with the maximum following the solar declination from $30^\circ N$ in winter to $45^\circ N$ in summer. Clearly eO3avi, even if scaled, is not a good surrogate for the impact of aviation on O_3 .

3.3. Burdens and lifetimes

The burden of excess tropospheric O_3 in Tg divided by the $100 \text{ Tg-O}_3 \text{ yr}^{-1}$ emissions defines the perturbation lifetime as given in Table 1 and shown in Figure 4. See also Figure A16 for the total excess burden and Figure A17 for separate plots of each experiment comparing tropospheric, stratospheric, and total burden. For experiment eNOavi, which does not have direct O_3 emissions, we

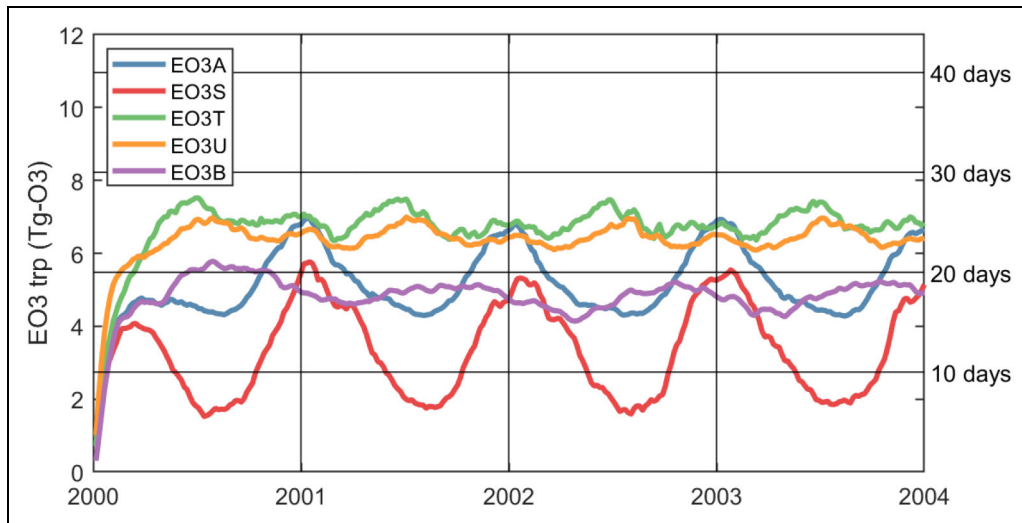


Figure 4. Tropospheric burden of excess O₃ (Tg) for the 5 experiments, showing 5-day intervals for years 2000 through 2003. The spin up in early 2000 is clearly visible. The lifetime scale (days, right axis) is calculated from the emission rate of 100 Tg-O₃ yr⁻¹ for both tropospheric and total burden, and it does not apply to eNO_{avi}. The legend notation is: EO3A = eO3avi; EO3S = eO3srf; EO3T = eO3ste1; EO3U = eO3ste2; EO3B = eNOavi.

cannot define a lifetime for the O₃ perturbation, so ignore the right axis. Both STE experiments (eO3ste1 and eO3ste2) are surprisingly similar in terms of tropospheric burden; both have similar lifetimes (approximately 25 days); and both show little seasonality. Aviation direct O₃ (eO3avi) is the next largest burden, but it shows large seasonality, accumulating more in northern winter. The surface O₃ (eO3srf) has the smallest burden and the largest seasonality in lifetime, from 6 days in summer to 21 days in winter. This sequence in lifetimes reflects the distance from emissions to photochemical sink, including surface deposition in these calculations. The sink in this case is the lower troposphere in the tropics or the summertime midlatitudes (see Figures 7 and 11 of Prather et al., 2023).

Excess O₃ peaks in January for eO3avi and eO3srf because there is a lower loss rate in the northern hemisphere (NH) winter. Such seasonality is unrealistic for typical pollution sources such as urban or aviation because the production of O₃ also drops substantially in winter. For eO3avi, the max:min (winter:summer) ratio of excess burden is 1.63, while for eNOavi, it is 1.22. The eNOavi excess burden is much less seasonal than that of eO3avi because the excess O₃ produced from aviation NO_x scales with O₃ loss and overall photochemical activity. We expect similar results for urban pollution (eO3srf) but could not define a simple emission scenario to test this.

3.4. Chemical modes and timescales

The steady-state patterns of O₃ perturbations are unique to each emission pattern (e.g. Figures 3 and A5–A9). The eO3avi/srf/ste1 zonal mean latitude-by-altitude patterns for July 1, 2003 and January 1, 2004 are shown in Figure A18; and these are the initial patterns just before our decay experiment in which we stop emissions. The subsequent decay of the NH tropospheric burden of excess O₃ is shown in Figure 5 (top), with the SH burden decay

shown in Figure A19. All excess burdens are scaled to a value of 1 at the start of decay, and the y-axis is logarithmic so that constant decay rates are straight lines. Constant decay lines of 10, 20, 30, and 40 days (left to right) are shown to guide the eye. In NH summer, the burdens start to decay with e-fold timescales between 10 and 20 days; while in winter the initial rate is much slower, 30–40 days. In NH summer, rates slow down (become flatter) after 2 months as we enter the fall; while in winter, they speed up (become steeper) as we enter the spring.

The surface emission patterns (eO3srf) start to decay more rapidly than the upper tropospheric patterns (eO3avi and eO3ste1) because more excess O₃ is near the surface where O₃ loss is more rapid from both chemistry and surface deposition. After a month or so, they tend to follow more parallel decay rates because the remaining O₃ is in a primary chemical mode with largest perturbations in the northern midlatitude upper troposphere. We can identify this primary O₃ mode, as the zonal mean altitude-by-latitude color maps in Figures 5 (bottom) and Figure A20. To calculate these modes, we drop the first month to allow short-term chemical modes to decay. These short-term modes will be primarily related to rapid transport of O₃ from the emission zone to neighboring regions. We then take the perturbation for days 30, 35, . . . , and 85 (months 2–3), scale each day's perturbation to a NH tropospheric O₃ perturbation of 5 Tg, and then average them. The patterns of excess O₃ for eO3avi, eO3srf, and eO3ste1 are remarkably similar and indicate that we have found the primary O₃ mode, at least for the midlatitudes. The timescales here of 10–40 days are similar to a range of intra-hemispheric transport and mixing scales, and there may be several overlapping modes in each hemisphere. We do not expect the emergence of a clean, single global mode as we found in similar experiments with N₂O and CH₄ (Hsu and Prather, 2010; Prather and Hsu, 2010).

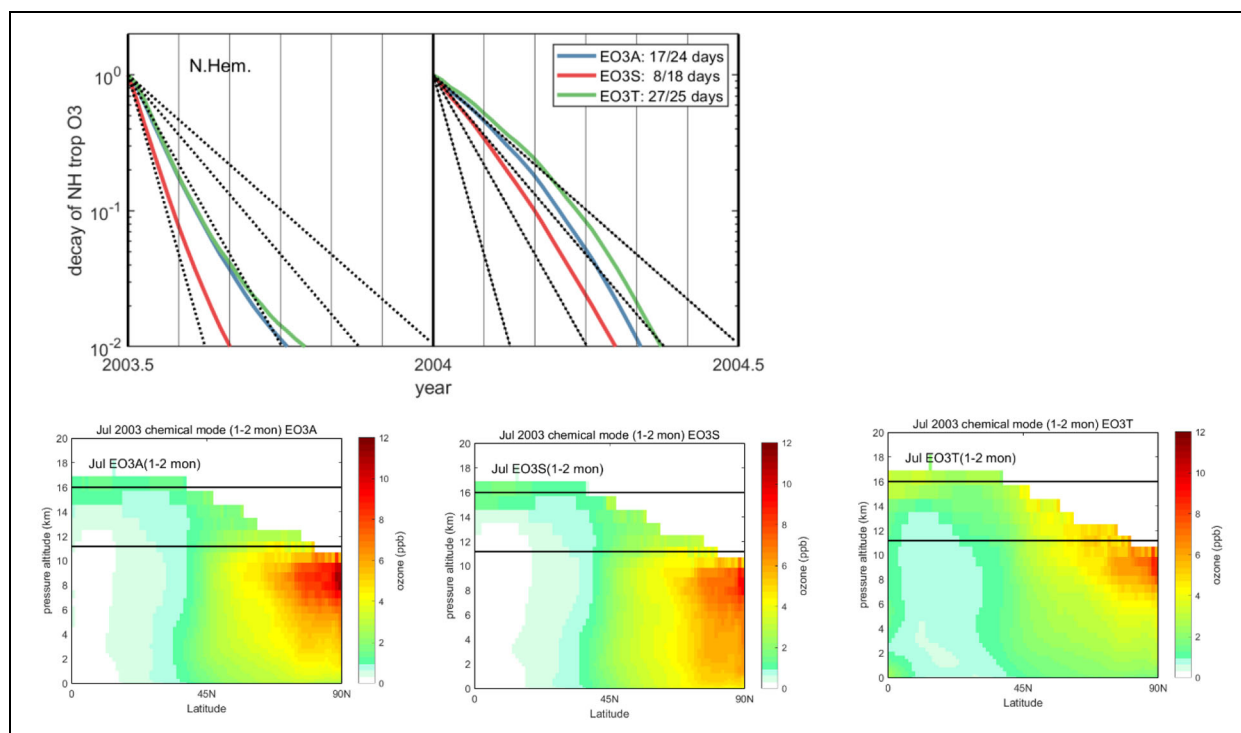


Figure 5. (top) Decay of northern hemisphere tropospheric O_3 perturbations for eO3avi/srf/ste1 (EO3A/S/T) rescaled to 1 at the time of cessation of emissions on July 1 (left) and January 1 (right). Dashed black lines are the same in both panels and show a constant decay of 10-, 20-, 30- and 40-day e-folds. The legend gives the min-to-max range in steady-state lifetime. Months are marked with vertical lines. (bottom) Chemical mode patterns for the troposphere following decay of eO3avi/srf/ste1 starting at July 1, 2003. Modes are calculated from averaged northern hemisphere (NH) patterns after 1–2 month decay (days 30–85). All perturbations are scaled to a total NH tropospheric O_3 perturbation of 5 Tg.

Table 2. Perturbation to key species as % in mass of CTRL for NH extratropics eO3avi on July 1, 2003

Pressure Range	O_3	HO_2	OH^a	NO_x	NO
200–600 hPa	+5.6%	+1.3%	–0.3%	–3.5%	–4.8%
600–1,000 hPa	+3.5%	+0.3%	+0.6%	–3.1%	–5.5%

Notes: Global tropospheric % change scaled by a factor of 4 to estimate the % change if all occurring in the northern extratropics ($30^\circ N$ – $90^\circ N$) where most of the O_3 perturbation occurs. OH^a is weighted by CH_4 loss. The excess O_3 loss that balances emissions (8.8 Tg for the month of July 2003) is about equally split between upper and lower troposphere. CTRL = control; NH = northern hemisphere.

3.5. Perturbations across other species

The emission-driven O_3 increases perturb all of tropospheric chemistry. In **Table 2** we present a brief summary of the relative changes in the northern extratropics for key species and rates from eO3avi on July 1, 2003. We find that most perturbations maximize in the upper troposphere (200–600 hPa) versus the lower troposphere (600–1000 hPa): +5.6% versus +3.5% for O_3 and –3.5% versus –3.1% for NO_x . The NO depletion is larger than that of NO_x and similar in both parts of the troposphere, about –5%, but still, NO_2 is depleted. The OH and HO_2 changes are more complex with HO_2 increasing and OH decreasing aloft, while both increasing near the surface. From the OH increase in the lower troposphere, the

global loss rate of CH_4 and CO to OH reactions increases, but by $\leq 0.1\%$.

The full latitude-by-altitude eO3avi patterns in % change for O_3 , NO , NO_2 , HNO_3 , PAN , CO , C_2H_6 , C_3H_8 , $HOOH$, CH_3OOH , and $HCHO$ are shown in Figure A21. The patterns here are consistent with the location of eO3avi emissions but are also related to the O_3 primary chemical mode (Figure A20). The O_3 increase is large (3%–5%) and extensive ($35^\circ N$ – $90^\circ N$, 6–11 km), and NO_x is reduced (1%–3%) over a similar domain. The OH radicals (not shown) are reduced, and thus the VOCs (CO , C_2H_6 , Alkane) increase by a fraction of 1%. The reduction in NO_x drives increased peroxides (H_2O_2 , CH_3OOH , PAN). Formaldehyde ($HCHO$) shows small, plus-minus changes indicating that

overall production of methyl radicals, a primary source of HCHO, is not changed. These patterns are probably similar for STE fluxes but may not apply to surface O₃ fluxes. The general concept that NO₂ is part of the O_x family and that an increase in O₃ would be accompanied by an increase in NO₂ is not borne out with a perturbation to O₃ in a full chemistry model.

4. Discussion and implications

4.1. Lifetimes

With these direct O₃ emission experiments, we are calculating a “perturbation lifetime,” that is, the excess burden of tropospheric O₃ divided by its emission rate. Lifetimes calculated here with the UCI CTM include chemical loss and surface (dry) deposition. Lifetimes vary seasonally, but fortunately with values <30 days, a steady state is reached for each season. This steady-state condition is critical because then the product of the lifetime times the 3D steady-state pattern are equivalent to the integral of impacts over the decay of a single-pulse emission, see theorem in Prather (2007). Calculation of perturbation lifetimes for tropospheric O₃ are rare (e.g., Figure 11 of Hsu and Prather [2009] estimates the lifetime from the slope of the tropospheric O₃ burden vs. the STE flux from a CTM experiment and gets 27–34 days). Most of the “lifetimes” we have discussed here are actually the inverse of the tropospheric mean loss frequency for O_x. Such lifetimes have no essential link to the chemical modes and timescales of the tropospheric O₃ system, yet their values are similar to the perturbation lifetimes. Is that fortuitous? or is there some underlying physics relating them? There are clearly problems with the inverse-loss lifetimes: they are singular in value; and they do not readily include the chemical feedbacks of O₃ on its production and loss. As a model metric for tropospheric O₃ that has followed the development of CCMs and CTMs for over 2 decades, the lifetime derived from LO_x remains an incredibly valuable diagnostic and its use should be continued with the same consistent definition (Equation 4), but it should not be confused with a true lifetime or used for timescales.

4.2. STE and tagged tracers

An obvious application of this work is a more accurate attribution of the role of STE on tropospheric O₃ and surface air quality. If we scale our eO₃ste experiments to an observation-based STE flux of about 400 Tg-O₃ yr⁻¹ (Murphy and Fahey, 1994; McLinden et al., 2000; Olsen et al., 2001; Ruiz and Prather, 2022), then a lifetime of 24 days scales to 26 TgO₃ or about 8% of the tropospheric burden. Even if we use the multimodel LO_x-based lifetime range of 24–32 days (Griffiths et al., 2021), and correct them for O₃ chemical feedbacks, we get similar results. So, what is wrong with the tagged tracer O₃S that measures stratospheric influence at about 40%? (Roelofs and Lelieveld, 1997; Williams et al., 2019; Abalos et al., 2020). The O₃S calculations use local values of $fO_{3,chem}^{LO_x}$ as the loss frequency, and we know that this underestimates the loss by 20%–40% because it fails to account for O₃ chemical feedbacks, but this is only a small fraction of the difference. This factor-of-5 difference in stratospheric influence

could be seen as simply definitional, but there are important implications for understanding future O₃. A number of model studies have estimated STE flux increases of up to 150 Tg-O₃ yr⁻¹ over the 21st century (Hegglin and Shepherd, 2009; Meul et al., 2018; Abalos et al., 2020; Wang and Fu, 2023). These models then exaggerate the resulting increase in tropospheric O₃ attributable to this STE flux as being 15% (50 Tg-O₃); whereas we would calculate that increase to be 3% (10 Tg-O₃). Fortunately, the models are calculating the “correct” overall tropospheric O₃ change for their CCM under scenario RCP-8.5 because the tagged tracer O₃S does not change the chemistry of O₃. Nevertheless, the attribution to the increased STE O₃ flux is misleading for policy use.

When we then try to attribute the O₃ changes to specific factors using a tagged O₃ tracer, we err. The fundamental problem is that O₃ and O₃S are interchangeable in terms of the chemistry and because O₃ is a dominant species, a perturbation to O₃S should be felt across all of tropospheric chemistry. Effectively, it increases the loss of the baseline O₃ which is not included with the tagged tracer experiment. A parallel case can be easily seen with CH₄. Assume that CH₄ has global lifetime of 9 years and a perturbation lifetime of 12 years. We add a small amount (1 Tg) of tagged CH₄ from riverine sources, CH₄R. The perturbation is small (0.02%) and so the OH lifetime perturbation is also small (approximately 0.006%). The tagged CH₄R will thus decay with a 9-year e-fold; however, we know that, and calculate that the overall 1 Tg perturbation to CH₄ decays with a 12-year e-fold. We can reconcile this conundrum by realizing that the perturbation caused by CH₄R is small but it applies to the entire CH₄ system, and thus it increases in the nontagged CH₄ that makes the perturbation decay with a 12-year e-fold. For O₃ and O₃S, the case is parallel but the chemical feedbacks are opposite: increased O₃ leads to more rapid O₃ loss and thus O₃S causes more rapid loss of total O₃ and its effective perturbation should decay more rapidly than the linear loss frequency used in O₃S experiments. The decay of the influence of STE is accurately modeled with a perturbation experiment as here.

4.3. Other chemical perturbations

Our experiments with 100 Tg annual emissions of tropospheric O₃ increase CH₄ loss via OH by about 0.08% (eO₃avi/srf) and 0.10% (eO₃ste1/ste2). eO₃avi/srf are slightly less effective because the impacts are mostly in NH midlatitudes, while most of the CH₄ is lost in the tropics favoring the STE fluxes of eO₃ste1/ste2. Aviation NO_x emissions that lead to a similar increase in O₃ have a much larger impact on CH₄ loss, +1.24%, because the NO_x shifts HO₂ into OH. Thus, we can attribute aviation's impact on tropospheric chemistry overall to the direct impact of NO_x emissions rather than to the secondary build-up of an O₃ perturbation, although the latter is a major component of aviation's climatic impact (Lee et al., 2020).

Comparing the build-up of O₃ as a secondary pollutant from aviation NO_x with that of the direct emissions, we find that the extra 0.85 Tg-N yr⁻¹ from eNO_{avi} produces

4.82 Tg excess O₃ at steady state, which is 91% of eO₃avi's perturbation and thus equivalent to 91 Tg-O₃ yr⁻¹. Converting to moles, we calculate an annual-mean ozone production efficiency (OPE) of 31 moles of O₃ produced per mole of NO emitted by aircraft, with a wintertime low of 24 on January 7 to a summertime high of 40 on July 1. This OPE estimate is only approximate because we use the perturbation lifetime from eO₃avi to scale the eNO_{avi} O₃ perturbation into a flux (Tg yr⁻¹). These values are consistent with OPE values for low-NO_x conditions in the free troposphere found in a variety of locations (Kleinman et al., 2002; Wild and Prather, 2006; Mazucca et al., 2016), and provide a novel way of calculating OPE. Nevertheless, the concept of an OPE is mainly heuristic, the impact of aviation can only be assessed from the excess O₃ calculated with an eNO_{avi} experiment.

4.4. Odd oxygen and family chemistry

The long-standing effort of the atmospheric chemistry community to group species into families has been productive, but for tropospheric O₃ this has reached new levels of complexity (Bates and Jacob, 2019; Archibald et al., 2020; Badia et al., 2021). A major goal in defining an O_x family is to describe a covarying set of species (like an eigenvector or chemical mode) whose net chemical reactions in and out can be used to estimate a loss frequency (like an eigenvalue). Yet to date, these efforts in abstracting tropospheric chemistry have not been able to address the nature of the chemical feedbacks. More complex definitions of odd oxygen have led to large increases in its lifetime that are simply not found in O₃ perturbation experiments. Further, a staple in the O_x family has always been NO₂, but we find that tropospheric O₃ perturbations are linked with decreases in NO₂, so that the family definition does not represent a fundamental chemical mode of the troposphere. This result was somewhat surprising and disappointing because O_x = O₃ + O is one of the chemical modes for Chapman chemistry in the stratosphere.

4.5. Remaining issues

How robust are the results here? We suspect they are within the 20% range that describes most of the differences across models (e.g., Stevenson et al., 2013; Young et al., 2018; Griffiths et al., 2021), including the UCI CTM. The results here do not depend on canceling effects, and the chemical perturbations and feedbacks driven by O₃ changes are straightforward and easy to assess.

Seasonality is a core element of the tropospheric O₃ budget, both production and loss, as found in the seasonality of the 4 Atom deployments (Prather et al., 2023). Fortunately, the O₃ timescales are much less than one season, a near steady state is reached within 1–2 months, and so one must consider separately the seasonal cycles in O₃ production or STE flux. For example, the wintertime accumulation of direct surface emissions (eO₃srf) fills the NH extratropical troposphere because O₃ loss is suppressed during NH winter. That pattern of excess O₃ is likely correct but the magnitude is exaggerated because surface production of secondary O₃ pollution drops off

outside of JJA. In the case of aviation, we directly diagnose a reduction in wintertime O₃ production with experiment eNO_{avi}, finding the accumulation of excess O₃ to be seasonally flat. Experiments like these, with simplified direct emissions, can be used in global chemistry models to diagnose the seasonal response of tropospheric O₃ perturbations to combined chemistry and transport. Direct perturbation experiments, either emission or pulse, also avoid the foibles of tagged tracers with incorrectly linearized chemistry, and they provide a more accurate assessment that includes full chemical feedbacks.

Data accessibility statement

The high-frequency 3-D datasets calculated with the UCI CTM and used in this study are provided in a Dryad archive (Prather, 2024). The Matlab scripts and a full set of .eps figures are provided in the parallel Zenodo archive.

Supplemental files

The supplemental files for this article can be found as follows:

Supplemental material as figures and tables are included as a pdf file.

Acknowledgments

The authors thank P. Griffiths and J. Keeble for helpful discussions during the formulation of this research, particularly for the efforts to design the next MIP focusing on atmospheric chemistry and the short-lived climate forcers.

Funding

Research at UCI was supported by grants NSF AGS-2135749 and NASA 80NSSC21K1454.

Competing interests

The authors declare that they have no competing interests.

Author contributions

Designed, drafted, and revised the paper: MJP.

Designed and performed the CTM calculations: XZ.

Analyzed the CTM data and prepared the figures and tables: MJP, XZ.

References

- Abalos, M, Orbe, C, Kinnison, DE, Plummer, D, Oman, LD, Jöckel, P, Morgenstern, O, Garcia, RR, Zeng, G, Stone, KA, Dameris, M. 2020. Future trends in stratosphere-to-troposphere transport in CCM1 models. *Atmospheric Chemistry and Physics* **20**(11): 6883–6901. DOI: <http://dx.doi.org/10.5194/acp-20-6883-2020>.
- Archibald, AT, Neu, JL, Elshorbany, Y, Cooper, OR, Young, PJ, Akiyoshi, H, Cox, RA, Coyle, M, Derwent, R, Deushi, M, Finco, A, Frost, GJ, Galbally, IE, Gerosa, G, Granier, C, Griffiths, PT, Hossaini, R, Hu, L, Jöckel, P, Josse, B, Lin, MY, Mertens, M, Morgenstern, O, Naja, M, Naik, V, Oltmans, S, Plummer, DA, Revell, LE, Saiz-Lopez, A, Saxena, P, Shin, YM, Shaahid, I, Shallcross, D, Tilmes, S,

- Trickl, T, Wallington, TJ, Wang, T, Worden, HM, Zeng, G.** 2020. Tropospheric ozone assessment report: A critical review of changes in the tropospheric ozone burden and budget from 1850 to 2100. *Elementa: Science of the Anthropocene* **8**: 1. DOI: <http://dx.doi.org/10.1525/elementa.2020.034>.
- Badia, A, Iglesias-Suarez, F, Fernandez, RP, Cuevas, CA, Kinnison, DE, Lamarque, J-F, Griffiths, PT, Tarasick, DW, Liu, J, Saiz-Lopez, A.** 2021. The role of natural halogens in global tropospheric ozone chemistry and budget under different 21st century climate scenarios. *Journal of Geophysical Research: Atmospheres* **126**(20): e2021JD034859. DOI: <http://dx.doi.org/10.1029/2021JD034859>.
- Bates, DR, Nicolet, M.** 1950. The photochemistry of atmospheric water vapour. *Journal of Geophysical Research* **55**(3): 301–327. DOI: <http://dx.doi.org/10.1029/JZ055i003p00301>.
- Bates, KH, Jacob, D.** 2019. An expanded definition of the odd oxygen family for tropospheric ozone budgets: Implications for ozone lifetime and stratospheric influence. *Geophysical Research Letters* **47**(4): e2019GL084486. DOI: <http://dx.doi.org/10.1029/2019GL084486>.
- Blum, HF.** 1959. *Carcinogenesis by ultraviolet light*. Princeton, NJ: Princeton University Press.
- Butler, JH.** 1994. The potential role of the ocean in regulating atmospheric CH₃Br. *Geophysical Research Letters* **21**(3): 185–188. DOI: <http://dx.doi.org/10.1029/94GL00071>.
- Chameides, W, Walker, JCG.** 1973. A photochemical theory of tropospheric ozone. *Journal of Geophysical Research* **78**(36): 8751–8760.
- Chapman, S.** 1930. A theory of upper-atmosphere ozone. *Memories of the Royal Metropolitan Society* **3**: 103–125.
- Danielsen, EF.** 1968. Stratospheric-tropospheric exchange based on radio-activity, ozone and potential vorticity. *Journal of the Atmospheric Sciences* **25**(3): 502–518. DOI: [http://dx.doi.org/10.1175/1520-0469\(1968\)025%3C0502:STEBOR%3E2.0.CO;2](http://dx.doi.org/10.1175/1520-0469(1968)025%3C0502:STEBOR%3E2.0.CO;2).
- Fishman, J, Crutzen, PJ.** 1978. The origin of ozone in the troposphere. *Nature* **274**: 855–858.
- Follows, MJ, Austin, JF.** 1992. A zonal average model of the stratospheric contributions to the tropospheric ozone budget. *Journal of Geophysical Research: Atmospheres* **97**(D16): 18047–18060. DOI: <http://dx.doi.org/10.1029/92JD01834>.
- Griffiths, PT, Murray, LT, Zeng, G, Shin, YM, Abraham, NL, Archibald, AT, Deushi, M, Emmons, LK, Galbally, IE, Hassler, B, Horowitz, LW, Keeble, J, Liu, J, Moeini, O, Naik, V, O'Connor, FM, Oshima, N, Tarasick, D, Tilmes, S, Turnock, ST, Wild, O, Young, PJ, Zanis, P.** 2021. Tropospheric ozone in CMIP6 simulations. *Atmospheric Chemistry and Physics* **21**(5): 4187–4218. DOI: <http://dx.doi.org/10.5194/acp-21-4187-2021>.
- Haagen-Smit, AJ.** 1952. Chemistry and physiology of Los Angeles smog. *Industrial and Engineering Chemistry* **44**(6): 1342–1346.
- Haagen-Smit, AJ, Fox, MM.** 1955. Automobile exhaust and ozone formation. *SAE Transactions* **63**: 575–580. Available at <https://www.jstor.org/stable/44468592>.
- Hegglin, MI, Shepherd, TG.** 2009. Large climate-induced changes in ultraviolet index and stratosphere-to-troposphere ozone flux. *Nature Geoscience* **2**(10): 687–691. DOI: <http://dx.doi.org/10.1038/ngeo604>.
- Holmes, CD, Prather, MJ, Søvde, AO, Myhre, G.** 2013. Future methane, hydroxyl, and their uncertainties: Key climate and emission parameters for future predictions. *Atmospheric Chemistry and Physics* **13**(1): 285–302. DOI: <http://dx.doi.org/10.5194/acp-13-285-2013>.
- Holmes, CD, Prather, MJ, Vinken, GCM.** 2014. The climate impact of ship NO_x emissions: An improved estimate accounting for plume chemistry. *Atmospheric Chemistry and Physics* **14**(13): 6801–6812. DOI: <http://dx.doi.org/10.5194/acp-14-6801-2014>.
- Hsu, J, Prather, MJ.** 2009. Stratospheric variability and tropospheric ozone. *Journal of Geophysical Research: Atmospheres* **114**(D6): 102. DOI: <http://dx.doi.org/10.1029/2008JD010942>.
- Hsu, J, Prather, MJ.** 2010. Global long-lived chemical modes excited in a 3-D chemistry transport model: Stratospheric N₂O, NO_y, O₃ and CH₄ chemistry. *Geophysical Research Letters* **37**(7): L07805. DOI: <http://dx.doi.org/10.1029/2009GL042243>.
- Isaksen, ISA, Hov, Ø.** 1987. Calculation of trends in the tropospheric concentration of O₃, OH, CO, CH₄ and NO_x. *Tellus B: Chemical and Physical Meteorology* **39**(3): 271–285. DOI: <http://dx.doi.org/10.3402/tellusb.v39i3.15347>.
- Johnston, HS.** 1971. Reduction of stratospheric ozone by nitrogen oxide catalysts from supersonic transport exhaust. *Science* **173**(3996): 517–522. DOI: <http://dx.doi.org/10.1126/science.173.3996.517>.
- Junge, CE.** 1962. Global ozone budget and exchange between stratosphere and troposphere. *Tellus* **14**(4): 363–377. DOI: <http://dx.doi.org/10.3402/tellusa.v14i4.9563>.
- Kleinman, LI, Daum, PH, Lee, Y-N, Nunnermacker, LJ, Springston, SR, Weinstein-Lloyd, J, Rudolph, J.** 2002. Ozone production efficiency in an urban area. *Journal of Geophysical Research: Atmospheres* **107**(D23): 4733. DOI: <http://dx.doi.org/10.1029/2002JD002529>.
- Lee, DS, Fahey, DW, Skowron, A, Allen, MR, Burkhardt, U, Chen, Q, Doherty, SJ, Freeman, S, Forster, PM, Fuglestvedt, J, Gettelman, A, De León, RR, Lim, LL, Lund, MT, Millar, RJ, Owen, B, Penner, JE, Pitari, G, Prather, MJ, Sausen, R, Wilcox, LJ.** 2020. The contribution of global aviation to anthropogenic climate forcing for 2000 to 2018. *Atmospheric Environment* **244**: 117834. DOI: <http://dx.doi.org/10.1016/j.atmosenv.2020.117834>.
- Levy, H II.** 1972. Photochemistry of the lower troposphere. *Planetary and Space Science* **20**(6): 919–935. DOI: [http://dx.doi.org/10.1016/0032-0633\(72\)90177-8](http://dx.doi.org/10.1016/0032-0633(72)90177-8).

- Logan, JA, Prather, MJ, Wofsy, SC, McElroy, MB.** 1981. Tropospheric chemistry: A global perspective. *Journal of Geophysical Research: Oceans* **86**(C8): 7210–7254. DOI: <http://dx.doi.org/10.1029/JC086iC08p07210>.
- Mazzuca, GM, Ren, X, Loughner, CP, Estes, M, Crawford, JH, Pickering, KE, Weinheimer, AJ, Dickerson, RR.** 2016. Ozone production and its sensitivity to NO_x and VOCs: Results from the DISCOVER-AQ field experiment, Houston 2013. *Atmospheric Chemistry and Physics* **16**(22): 14463–14474. DOI: <http://dx.doi.org/10.5194/acp-16-14463-2016>.
- McLinden, C, Olsen, S, Hannegan, B, Wild, O, Prather, M, Sundet, J.** 2000. Stratospheric ozone in 3-D models: A simple chemistry and the cross-tropopause flux. *Journal of Geophysical Research: Atmospheres* **105**(D11): 14653–14665.
- Meul, S, Langematz, U, Kröger, P, Oberländer-Hayn, S, Jöckel, P.** 2018. Future changes in the stratosphere-to-troposphere ozone mass flux and the contribution from climate change and ozone recovery. *Atmospheric Chemistry and Physics* **18**(10): 7721–7738. DOI: <http://dx.doi.org/10.5194/acp-18-7721-2018>.
- Molina, MJ, Rowland, FS.** 1974. Stratospheric sink for chlorofluoromethanes: Chlorine atom-catalysed destruction of ozone. *Nature* **249**: 810–812. DOI: <http://dx.doi.org/10.1038/249810a0>.
- Murphy, DM, Fahey, DW.** 1994. An estimate of the flux of stratospheric reactive nitrogen and ozone into the troposphere. *Journal of Geophysical Research: Atmospheres* **99**(D3): 5325–5332.
- Nicolet, M.** 1975. Stratospheric ozone: An introduction to its study. *Reviews of Geophysics* **13**(5): 593–636. DOI: <http://dx.doi.org/10.1029/RG013i005p00593>.
- Olsen, SC, McLinden, CA, Prather, MJ.** 2001. The stratospheric NO_y-N₂O system: Testing uncertainties in a 3-D framework. *Journal of Geophysical Research: Atmospheres* **106**(D22): 28771–28784.
- Prather, MJ.** 1994. Lifetimes and eigenstates in atmospheric chemistry. *Geophysical Research Letters* **21**(9): 801–804. DOI: <http://dx.doi.org/10.1029/94GL00840>.
- Prather, MJ.** 1996. Natural modes and time scales in atmospheric chemistry: Theory, GWPs for CH₄ and CO, and runaway growth. *Geophysical Research Letters* **23**(19): 2597–2600. DOI: <http://dx.doi.org/10.1029/96GL02371>.
- Prather, MJ.** 1997. Time scales in atmospheric chemistry: CH₃Br, the ocean, and ODPs. *Global Biogeochemical Cycles* **11**(3): 393–400. DOI: <http://dx.doi.org/10.1029/97GB01055>.
- Prather, MJ.** 2007. Lifetimes and time scales in atmospheric chemistry. *Philosophical Transactions of the Royal Society A* **365**(1856): 1705–1726. DOI: <http://dx.doi.org/10.1098/rsta.2007.2040>.
- Prather, M.** 2024. Lifetimes and timescales of tropospheric ozone: Ozone emission experiments [Dataset]. Dryad. DOI: <http://dx.doi.org/10.5061/dryad.qbzkh18qq>.
- Prather, MJ, Ehhalt, D, Dentener, F, Derwent, R, Dlugokencky, E, Holland, E, Isaksen, I, Karima, J, Kirchhoff, V, Matson, P.** 2001. Atmospheric chemistry and greenhouse gases, in Houghton, JT, Ding, Y, Griggs, DJ, Noguer, M, van der Linden, PJ, Daix, PJ, Maskell, K, Johnson, CA eds., *Climate change 2001: The scientific basis. Contribution of Working Group I to the Third Assessment Report of the Intergovernmental Panel on Climate Change*. Cambridge, UK: Cambridge University Press: 239–289.
- Prather, MJ, Guo, H, Zhu, X.** 2023. Deconstruction of tropospheric chemical reactivity using aircraft measurements: The Atmospheric Tomography Mission (ATom) data. *Earth System Science Data* **15**(7): 3299–3349. DOI: <http://dx.doi.org/10.5194/essd-15-3299-2023>.
- Prather, MJ, Hsu, J.** 2010. Coupling of nitrous oxide and methane by global atmospheric chemistry. *Science* **330**(6006): 952–954. DOI: <http://dx.doi.org/10.1126/science.1196285>.
- Prather, MJ, Zhu, X, Flynn, CM, Strode, SA, Rodriguez, JM, Steenrod, SD, Liu, J, Lamarque, J-F, Fiore, AM, Horowitz, LW, Mao, J, Murray, LT, Shindell, DT, Wofsy, SC.** 2017. Global atmospheric chemistry—Which air matters. *Atmospheric Chemistry and Physics* **17**(14): 9081–9102. DOI: <http://dx.doi.org/10.5194/acp-17-9081-2017>.
- Prather, MJ, Zhu, X, Tang, Q, Hsu, J, Neu, JL.** 2011. An atmospheric chemist in search of the tropopause. *Journal of Geophysical Research: Atmospheres* **116**(D4): D04306. DOI: <http://dx.doi.org/10.1029/2010JD014939>.
- Roelofs, GJ, Lelieveld, J.** 1997. Model study of the influence of cross-tropopause O₃ transports on tropospheric O₃ levels. *Tellus B* **49**(1): 38–55. DOI: <http://dx.doi.org/10.3402/tellusb.v49i1.15949>.
- Roffo, AH.** 1939. Ueber die physikalisch-chemische Aetologie der Krebskrankheit. *Strahlentherapie* **66**: 328–350.
- Ruiz, DJ, Prather, MJ.** 2022. From the middle stratosphere to the surface, using nitrous oxide to constrain the stratosphere–troposphere exchange of ozone. *Atmospheric Chemistry and Physics* **22**(3): 2079–2093. DOI: <http://dx.doi.org/10.5194/acp-22-2079-2022>.
- Stevenson, DS, Young, PJ, Naik, V, Lamarque, JF, Shindell, DT, Voulgarakis, A, Skeie, RB, Dalsoren, SB, Myhre, G, Berntsen, TK, Folberth, GA, Rumbold, ST, Collins, WJ, MacKenzie, IA, Doherty, RM, Zeng, G, van Noije, TPC, Strunk, A, Bergmann, D, Cameron-Smith, P, Plummer, DA, Strode, SA, Horowitz, L, Lee, YH, Szopa, S, Sudo, K, Nagashima, T, Josse, B, Cionni, I, Righi, M, Eyring, V, Conley, A, Bowman, KW, Wild, O, Archibald, A.** 2013. Tropospheric ozone changes, radiative forcing and attribution to emissions in the Atmospheric Chemistry and Climate Model Intercomparison Project (ACCMIP). *Atmospheric Chemistry and Physics* **13**(6): 3063–3085. DOI: <http://dx.doi.org/10.5194/acp-13-3063-2013>.

- Szopa, S, Naik, V, Adhikary, B, Artaxo, P, Bernsten, T, Collins, WD, Fuzzi, S, Gallardo, L, Kiendler-Scharr, A, Klimont, Z, Liao, H, Unger, N, Zanis, P.** 2021. Short-lived climate forcers, in Masson-Delmotte, V, Zhai, P, Pirani, A, Connors, SL, Péan, PC, Berger, S, Caud, N, Chen, Y, Goldfarb, L, Gomis, MI, Huang, M, Leitzell, K, Lonnoy, E, Matthews, JBR, Maycock, JBR, Maycock, TK, Waterfield, T, Yelekçi, O, Yu, R, Zhou, B eds., *Climate Change 2021: The Physical Science Basis. Contribution of Working Group I to the Sixth Assessment Report of the Intergovernmental Panel on Climate Change*. Cambridge, UK; New York, NY: Cambridge University Press: 817–922. DOI: <http://dx.doi.org/10.1017/9781009157896.008>.
- Tang, Q, Prather, MJ.** 2012. Five blind men and the elephant: What can the NASA Aura ozone measurements tell us about stratosphere-troposphere exchange? *Atmospheric Chemistry and Physics* **12**(5): 2357–2380. DOI: <http://dx.doi.org/10.5194/acp-12-2357-2012>.
- Thrush, BA.** 1980. The chemistry of the stratosphere. *Philosophical Transactions of the Royal Society A: Mathematical, Physical and Engineering Sciences* **296**(1418): 149–160. DOI: <https://doi.org/10.1098/rsta.1980.0161>.
- Wang, M, Fu, Q.** 2023. Changes in stratosphere-troposphere exchange of air mass and ozone concentration in CCMI models from 1960 to 2099. *Journal of Geophysical Research: Atmospheres* **128**(13): e2023JD038487. DOI: <http://dx.doi.org/10.1029/2023JD038487>.
- Wild, O, Prather, MJ.** 2006. Global tropospheric ozone modeling: Quantifying errors due to grid resolution. *Journal of Geophysical Research: Atmospheres* **111**(D11): D11305. DOI: <http://dx.doi.org/10.1029/2005JD006605>.
- Wild, O, Sundet, JK, Prather, MJ, Isaksen, ISA, Aki-moto, H, Browell, EV, Oltmans, SJ.** 2003. Chemical transport model ozone Simulations for spring 2001 over the western Pacific: Comparisons with TRACE-P lidar, ozonesondes and Total Ozone Mapping Spectrometer columns. *Journal of Geophysical Research: Atmospheres* **108**(D21): 8826. DOI: <http://dx.doi.org/10.1029/2002JD003283>.
- Williams, RS, Hegglin, MI, Kerridge, BJ, Jöckel, P, Latter, BG, Plummer, DA.** 2019. Characterising the seasonal and geographical variability in tropospheric ozone, stratospheric influence and recent changes. *Atmospheric Chemistry and Physics* **19**(6): 3589–3620. DOI: <http://dx.doi.org/10.5194/acp-19-3589-2019>.
- World Meteorological Organization.** 2022. Scientific Assessment of Ozone Depletion: 2022 Executive Summary. GAW Report No. 278. Geneva, Switzerland: WMO: 56. Available at <https://library.wmo.int/idurl/4/42105>. Accessed August 28, 2023.
- Young, PJ, Naik, V, Fiore, AM, Gaudel, A, Guo, J, Lin, MY, Neu, JL, Parrish, DD, Rieder, HE, Schnell, JL, Tilmes, S, Wild, O, Zhang, L, Ziemke, J, Brandt, J, Delcloo, A, Doherty, RM, Geels, C, Hegglin, MI, Hu, L, Im, U, Kumar, R, Luhar, A, Murray, L, Plummer, D, Rodriguez, J, Saiz-Lopez, A, Schultz, MG, Woodhouse, MT, Zeng, G.** 2018. Tropospheric Ozone Assessment Report: Assessment of global-scale model performance for global and regional ozone distributions, variability, and trends. *Elementa: Science of the Anthropocene* **6**: 10. DOI: <http://dx.doi.org/10.1525/elementa.265>.
- Ziemke, JR, Chandra, S.** 2012. Development of a climate record of tropospheric and stratospheric column ozone from satellite remote sensing: Evidence of an early recovery of global stratospheric ozone. *Atmospheric Chemistry and Physics* **12**(13): 5737–5753. DOI: <https://doi.org/10.5194/acp-12-5737-2012>.
- Ziemke, JR, Chandra, S, Duncan, BN, Froidevaux, L, Bhartia, PK, Levelt, PF, Waters, JW.** 2006. Tropospheric ozone determined from Aura OMI and MLS: Evaluation of measurements and comparison with the Global Modeling Initiative's Chemical Transport Model. *Journal of Geophysical Research: Atmospheres* **111**(D19): D19303. DOI: <http://dx.doi.org/10.1029/2006JD007089>.

How to cite this article: Prather, MJ, Zhu, X. 2024. Lifetimes and timescales of tropospheric ozone. *Elementa: Science of the Anthropocene* 12(1). DOI: <https://doi.org/10.1525/elementa.2023.00112>

Domain Editor-in-Chief: Detlev Helmig, Boulder AIR LLC, Boulder, CO, USA

Associate Editor: Alastair Lewis, National Centre for Atmospheric Science, University of York, York, UK

Knowledge Domain: Atmospheric Science

Part of an Elementa Special Feature: Tropospheric Ozone Assessment Report (TOAR): Global Metrics for Climate Change, Human Health, and Crop/Ecosystem Research

Published: February 29, 2024 **Accepted:** December 22, 2023 **Submitted:** August 22, 2023

Copyright: © 2024 The Author(s). This is an open-access article distributed under the terms of the Creative Commons Attribution 4.0 International License (CC-BY 4.0), which permits unrestricted use, distribution, and reproduction in any medium, provided the original author and source are credited. See <http://creativecommons.org/licenses/by/4.0/>.



Elem Sci Anth is a peer-reviewed open access journal published by University of California Press.

OPEN ACCESS 

APPENDIX: Lifetimes and timescales of tropospheric ozone

Michael J. Prather and Xin Zhu

TABLES

Table A1. Chemistry in the UCI CTM

Table A2. Emissions & Boundary Conditions for these experiments

Table A3. UCI CTM References

FIGURES

Figure A1. Stratospheric zonal mean O₃ abundance (ppm) averaged over four seasons (DJF, MAM, JJA, SON) comprised of 5-day snapshots from year 2003 of the CTRL run. Coordinates are latitude by pressure altitude $z^* = 16 \text{ km} \log_{10}(1/P(\text{bars}))$ and assume a surface pressure everywhere of 1 bar.

Figure A2. Tropospheric zonal mean O₃ abundance (ppb), see Fig. A1. Some pixels in Fig. A1 and A2 contain both stratospheric and tropospheric values because the pixel contained was both stratospheric and tropospheric air over the 18 snapshots and 320 longitude cells (e.g., stratospheric intrusions).

Figure A3. Stratospheric (top) and tropospheric (bottom) global mean O₃ columns (DU) from the CTRL run calculated from the 365 5-day snapshots over the five years, 2000 through 2004.

Figure A4. Perturbation in the O₃ column (DU) for eO₃avi (top), eO₃srf (middle), and eO₃ste1 (bottom), separating troposphere (blue) from stratosphere (red). Also shown are the decay of the perturbations following cessation of emissions on July 1 (2003.5) and Jan 1 (2004.0). In terms of DU, the annual emissions $100 \text{ Tg-O}_3/\text{y} = 9.2 \text{ DU}/\text{y}$, and thus a tropospheric perturbation of 0.5 DU has a lifetime of 20 days.

Figure A5. eO₃avi perturbation to zonal mean O₃ abundance (ppb) for four seasons (DJF, MAM, JJA, SON), split into stratospheric (top panels) and tropospheric (bottom panels). For methodology, see Figure A1. Aviation emissions (eO₃avi) occur mostly in the northern troposphere but reach into the stratosphere and southern hemisphere. Note that color bars have the same range on all plots.

Figure A6. eNO₃avi perturbation to zonal mean O₃ abundance (ppb) for four seasons (DJF, MAM, JJA, SON), split into stratospheric (top panels) and tropospheric (bottom panels). For methodology, see Figure A1. For eNO₃avi, aviation emissions of NO_x are doubled. Note that color bars have the same range on all plots.

Figure A7. eO₃srf perturbation to zonal mean O₃ abundance (ppb) for four seasons (DJF, MAM, JJA, SON), split into stratospheric (top panels) and tropospheric (bottom panels). For methodology, see Figure A1. Surface emissions (eO₃srf) occur within the black square over a limited longitude range, see Table 1.

Figure A8. eO₃ste1 perturbation to zonal mean O₃ abundance (ppb) for four seasons (DJF, MAM, JJA, SON), split into stratospheric (top panels) and tropospheric (bottom panels). For methodology, see Figure A1. STE emissions (eO₃ste1) occur within the black squares equally in each hemisphere and across all longitudes, see Table 1.

Figure A9. eO3ste2 perturbation to zonal mean O₃ abundance (ppb) for four seasons (DJF, MAM, JJA, SON), split into stratospheric (top panels) and tropospheric (bottom panels). For methodology, see Figure A1. STE emissions (eO3ste2) occur within the black squares equally in each hemisphere and across all longitudes, see Table 1.

Figure A10. Stratospheric (top) and tropospheric (bottom) O₃ column (DU) for year 2003 from the control (CTRL) simulation. Columns are a function of latitude and time at 5-day intervals.

Figure A11. Ozone column perturbation (DU) for experiment eO3avi (aviation O₃) as a function of latitude and time (2000.0 to 2004.0) at 5-day intervals for stratosphere (top) and troposphere (bottom).

Figure A12. Ozone column perturbation (DU) for experiment eNOavi (aviation NO_x) as a function of latitude and time (2000.0 to 2004.0) at 5-day intervals for stratosphere (top) and troposphere (bottom).

Figure A13. Ozone column perturbation (DU) for experiment eO3srf (surface O₃) as a function of latitude and time (2000.0 to 2004.0) at 5-day intervals for stratosphere (top) and troposphere (bottom).

Figure A14. Ozone column perturbation (DU) for experiment eO3ste1 (STE O₃) as a function of latitude and time (2000.0 to 2004.0) at 5-day intervals for stratosphere (top) and troposphere (bottom).

Figure A15. Ozone column perturbation (DU) for experiment eO3ste2 (STE O₃) as a function of latitude and time (2000.0 to 2004.0) at 5-day intervals for stratosphere (top) and troposphere (bottom).

Figure A16. Total (top) and tropospheric (bottom) burden of excess O₃ (Tg) for the five experiments, showing 5-day intervals for years 2000 through 2003. The spin up in early 2000 is clearly visible. The lifetime scale (days, right axis) is calculated from the emission rate of 100 Tg-O₃ yr⁻¹ for both tropospheric and total burden, and it does not apply to eNOavi (EO3B).

Figure A17. Burden of excess O₃ (Tg) for the five experiments: eO3avi (EO3A), eNOavi (EO3B), eO3ste1 (EO3T), eO3ste2 (EO3U), and eO3srf (EO3S). For each experiment, the tropospheric (dashed line), stratospheric (dotted line) and total (solid line) are shown. See Figure A16.

Figure A18. Instantaneous patterns of NH tropospheric O₃ perturbation for eO3avi/srf/ste1 at 1 Jul 2003 and 1 Jan 2004. All patterns are scaled to a total of 5 Tg.

Figure A19. (top) Decay of northern hemisphere tropospheric O₃ perturbations for eO3avi/srf/ste1 rescaled to 1 at the time of cessation of emission on July 1 (left) and January 1 (right). Dashed black lines are the same in both panels and show a constant decay of 10-, 20-, 30- and 40-day e-folds. The legend gives the min-to-max range in steady-state lifetime. Months are marked with vertical lines. (bottom) Same plot for southern hemisphere tropospheric O₃.

Figure A20. Chemical mode patterns for the troposphere following decay of eO3avi/srf/ste1 starting at 1 Jul 2003 and 1 Jan 2004. Modes are calculated from averaged NH patterns after 1-2 months of decay (days 30-85). All perturbations are scaled to a total NH tropospheric O₃ perturbation of 5 Tg.

Figure A21. Latitude-by-altitude plots of the perturbations to key chemical species for the eO3avi (aviation) vs. CTRL on 1 Jul 2003. The upper-left-corner panel shows the O₃ perturbation in ppb to compare with earlier figures. All other panels, including the 2nd O₃ panel are in % difference. Note that the color bar, -3% to +3%, is the same for all the relative change panels.

Table A1. Chemistry and Transport in the UCI CTM

Tropospheric Chemical Species							
O(¹ D)*	OH [^]	O ₃	HO ₂	NO	NO ₂	NO ₃	N ₂ O ₅
HNO ₃	HNO ₄	H ₂ O ₂	CH ₃ OO	CH ₃ OOH	H ₂ CO	C ₂ H ₅ OO	C ₂ H ₅ OOH
C ₂ H ₄ O	C ₂ H ₃ O ₃	PAN	Alkene	Alkane [#]	C ₂ H ₆ [#]	CH ₄ [#]	CO [#]
H ₂ [#]	C ₅ H ₈	C ₄ H ₆ O	C ₅ H ₇ O ₂ [^]	C ₄ H ₅ O ₃ [^]	ROHO ₂ [^]	C ₃ H ₆ O ^{&}	H ₂ O ^{&}
e90 [%]							
All species included as implicit chemistry and transport EXCEPT: * = instant steady state; ^ = transported with +parent molecule (see below); # = explicit chemistry; & = specified abundance; % = no chemistry, 90-day e-fold.							
Key: C ₂ H ₄ O = Acetaldehyde; C ₂ H ₃ O ₃ = Peroxyacetyl radical; PAN = C ₂ H ₃ O ₃ NO ₂ = Peroxyacetyl nitrate; Alkene = C ₃ H ₆ + other alkene emissions; Alkane = C ₃ H ₈ + higher alkane emissions; C ₅ H ₈ = Isoprene; C ₄ H ₆ O = Methacrolein or Methyl vinyl ketone; C ₅ H ₇ O ₂ = Isoprene peroxy radical (all types); C ₄ H ₅ O ₃ = Methyl vinyl ketone peroxy radicals (all types); ROHO ₂ = C ₃ H ₇ O ₃ = Hydroxypropanyl peroxy radical formed from Alkene + OH; C ₃ H ₆ O = Acetone.							
Transported pairs, for the chemistry initialize: OH as 1% of HO ₂ ; ROHO ₂ as 0.1% of Alkene; C ₅ H ₇ O ₂ as 0.1% of C ₅ H ₈ ; C ₄ H ₅ O ₃ as 0.1% of C ₄ H ₆ O.							
Stratospheric Chemical Species							
O ₃	N ₂ O	CH ₄	NO _y				
Notes: NO _y = NO + NO ₂ + NO ₃ + 2 N ₂ O ₅ + HNO ₃ + HNO ₄ + PAN							
Tracer Transport							
source	ECMWF IFS cycle 38r1 3-hr averaged forecasts (winds, convection, temperature, q, rain, clouds)						
resolution	native resolution T159L60 (1.1° x 1.1°, 34 layers in troposphere)						
numerics	second-order moments for tracers, fractional overlap for clouds and washout, explicit STE fluxes						

Table A2. Emissions & Boundary Conditions

Species	Tg-species per year	Notes
NO	88.2 + 10.7	Lightning NO _x tuned to 5 TgN = 10.7 TgNO as multi-year average
NO ₂	0.1	
H ₂ CO	14.4	
CO	1274.4	
C ₂ H ₆	7.8	
C ₂ H ₄ O	23.5	
Alkane	49.1	
Alkene	66.9	
Isoprene	523.4	
e90	2073.8	Globally uniform surface, tuned to give 100 ppb at steady state

Emission Source	Reference	Species
Anthropogenic surface	RCP 6.0 year 2000	NO, CO, C ₂ H ₆ , Alkane, Alkene, H ₂ CO, C ₂ H ₄ O
Aviation NO _x	RCP 6.0 year 2000	NO (96%), NO ₂ (4%)
Biomass burning	GFED4 year 1997	NO, CO, C ₂ H ₆ , Alkane, Alkene, H ₂ CO, C ₂ H ₄ O
Biogenics	MEGAN 2.1	CO, Alkene, H ₂ CO, C ₂ H ₄ O, C ₅ H ₈
Lightning NO _x	Holmes++ 2013, 2104	NO

Species	Fixed abundance	Notes
CH ₄	LBC: SH-NH = 1750-1850 ppb	
N ₂ O	LBC: SH-NH = 316-316 ppb	
H ₂	LBC: SH-NH = 550-500 ppb	
C ₃ H ₆ O	All trop: 90S-60S-30S-20S-20N-30N-60N-90N = 150-250-350-500-700-900-700 ppt	From ATom, uniform in vertical = 200-200-200-400-600-600-600 ppt

Table A3. UCI CTM References documenting application and development of UCI CTM and its components. This chemistry-transport model began as a Harvard & GISS joint enterprise, and then moved to UC Irvine. The meteorological fields used in the CTM were originally from the GISS GCM developed by Gary Russell (11-layer tropospheric model and 21-layer stratospheric model). In the late 1990s Jostein Sundet visited UCI and developed the next generation of meteorological fields based on the ECMWF IFS that U. Oslo had access to. The tropospheric chemistry was initially built by Oliver Wild while at FRSGC Yokohama and thus also known as FRSGC CTM. After 1992, most all of the lead authors on these papers were graduate students, post-docs, or visitors in the Earth System Science Department at UC Irvine.

1. Sand, Maria, R. B. Skeie, M. Sandstad, S. Krishnan, G. Myhre, H. Bryant, R. Derwent, D. Hauglustaine, F. Paulot, M. Prather & D. Stevenson (2023) A multi-model assessment of the Global Warming Potential of hydrogen, *Nature Communications: Earth & Environment*, 4:203, doi: 10.1038/s43247-023-00857-8.
2. Prather, M. J. (2022) CO₂ surface variability: from the stratosphere or not?, *Earth Syst. Dynam.*, 13, 703–709, doi: 10.5194/esd-13-703-2022.
3. Ruiz, D. J. and M.J. Prather (2022) From the middle stratosphere to the surface, using nitrous oxide to constrain the stratosphere–troposphere exchange of ozone, *Atmos. Chem. Phys.*, 22, 2079–2093, doi: 10.5194/acp-22-2079-2022.
4. Ruiz, Daniel J., Michael J. Prather, Susan E. Strahan, Rona L. Thompson, Lucien Froidevaux, Stephen D. Steenrod (2021), How atmospheric chemistry and transport drive surface variability of N₂O and CFC-11. *J. Geophys. Res.: Atmospheres*, 126, e2020JD033979, doi: 10.1029/2020JD033979.
5. Nicewonger, M. R., Aydin, M., Prather, M. J., & Saltzman, E. S. (2020). Extracting a history of global fire emissions for the past millennium from ice core acetylene, ethane, and methane, *J. Geophys. Res.-Atmos.* 125 (20), e2020JD032932.
6. Nicewonger, M. R., Aydin, M., Prather, M. J., & Saltzman, E. S. (2020). Reconstruction of paleofire emissions over the past millennium from measurements of ice core acetylene. *Geophysical Research Letters*, 47, e2019GL085101. doi.org/10.1029/2019GL085101.
7. Prather, M.J. and J.C. Hsu (2019) A round Earth for climate models, *Proc Natl Acad Sci*, 116 (39) 19330–19335; <https://doi.org/10.1073/pnas.1908198116>.
8. Nicewonger, M.R., M. Aydin, M.J. Prather, E.S. Saltzman, (2018) Large changes in biomass burning over the last millennium inferred from paleoatmospheric ethane in polar ice cores, *PNAS*, 115 (49), 12413–12418, doi: 10.1073/pnas.1807172115.
9. Hall, Samuel R., Kirk Ullmann, Michael J. Prather, Clare M. Flynn, Lee T. Murray, Arlene M. Fiore, Gustavo Correa, Sarah A. Strode, Stephen D. Steenrod, Jean-Francois Lamarque, Jonathon Guth, Béatrice Josse, Johannes Flemming, Vincent Huijnen, N. Luke Abraham, and Alex T. Archibald (2018) Cloud impacts on photochemistry: a new climatology of photolysis rates from the Atmospheric Tomography mission, *Atmos. Chem. Phys.*, 18, 16809–16828, doi: 10.5194/acp-18-16809-2018.
10. Prather, M.J., Clare M. Flynn, Xin Zhu, Stephen D. Steenrod, Sarah A. Strode, Arlene M. Fiore, Gustavo Correa, Lee T. Murray, and Jean-Francois Lamarque (2018) How well can global chemistry models calculate the reactivity of short-lived greenhouse gases in the remote troposphere, knowing the chemical composition, *Atmos. Meas. Tech.*, 11, 2653–2668, 2018, doi: 10.5194/amt-11-2653-2018.
11. Prather, M.J., Xin Zhu, Clare M. Flynn, Sarah A. Strode, Jose M. Rodriguez, Stephen D. Steenrod, Junhua Liu, Jean-Francois Lamarque, Arlene M. Fiore, Larry W. Horowitz, Jingqiu Mao, Lee T. Murray, Drew T. Shindell, and Steven C. Wofsy (2017) Global Atmospheric Chemistry – Which Air Matters, *Atmos. Chem. Phys.*, 17(14), 9081–9102, doi: 10.5194/acp-17-9081-2017.
12. Prather, M.J. (2015) Photolysis rates in correlated overlapping cloud fields: Cloud-J 7.3c, *Geosci. Model Dev.*, 8, 2587–2595, doi:10.5194/gmd-8-2587-2015.
13. Prather, M.J., J. Hsu, N.M. DeLuca, C.H. Jackman, L.D. Oman, A.R. Douglass, E.L. Fleming, S.E. Strahan, S.D. Steenrod, O.A. Søvde, I.S.A. Isaksen, L. Froidevaux, and B. Funke (2015) Measuring and modeling the lifetime of nitrous oxide including its variability, *J. Geophys. Res. Atmos.*, 120, 5693–5705. doi: 10.1002/2015JD023267.

14. Hsu, Juno and M.J. Prather (2014) Is the vertical residual velocity a good proxy for stratosphere-troposphere exchange of ozone? *Geophys. Res. Lett.*, 41, doi:10.1029/2014GL061994
15. Schnell, J.L., C. D. Holmes, A. Jangam, M. J. Prather (2014) Skill in forecasting extreme ozone pollution episodes with a global atmospheric chemistry model, *Atmos. Chem. Phys.*, 14, 7721–7739, doi:10.5194/acp-14-7721-2014.
16. Holmes, C.D., M. J. Prather, and G. C. M. Vinken (2014) The climate impact of ship NO_x emissions: an improved estimate accounting for plume chemistry, *Atmos. Chem. Phys.*, 14, 6801–6812, doi:10.5194/acp-14-6801-2014
17. Lauritzen, P.H., P.A. Ullrich, C. Jablonowski, P. A. Bosler, D. Calhoun, A.J. Conley, T. Enomoto, L. Dong, S. Dubey, O. Guba, A.B. Hansen, E. Kaas, J. Kent, J.-F. Lamarque, M.J. Prather, D. Reinert, V.V. Shashkin, W.C. Skamarock, B. Sørensen, M.A. Taylor, and M.A. Tolstykh (2014) A standard test case suite for two-dimensional linear transport on the sphere: results from a collection of state-of-the-art schemes, *Geosci. Model Dev.*, 7, 105–145, doi:10.5194/gmd-7-105-2014.
18. Hsu, Juno, M.J. Prather, D. Bergmann, P. Cameron-Smith (2013), Sensitivity of stratospheric dynamics to uncertainty in O₃ production, *J. Geophys. Res. Atmos.*, 118, 8984–8999, doi:10.1002/jgrd.50689.
19. Holmes, C.D., M. J. Prather, A.O. Søvde, G. Myhre (2013) Future methane, hydroxyl, and their uncertainties: key climate and emission parameters for future predictions, *Atmos. Chem. Phys.*, 13, 285–302, doi:10.5194/acp-13-285-2013
20. Tang, Qi and M. J. Prather (2012), Tropospheric column ozone: matching individual profiles from Aura OMI and TES with a chemistry-transport model, *Atmos. Chem. Phys.*, 12, 10441-10452, doi:10.5194/acp-12-10441-2012.
21. Tang, Qi and M.J. Prather (2012), Five blind men and the elephant: what can the NASA Aura ozone measurements tell us about stratosphere-troposphere exchange? *Atmos. Chem. Phys.*, 12, 2357–2380, doi:10.5194/acp-12-2357-2012.
22. Neu, J.L. and M. J. Prather (2012), Toward a more physical representation of precipitation scavenging in global chemistry models: cloud overlap and ice physics and their impact on tropospheric ozone, *Atmos. Chem. Phys.*, 12, 3289-3310, doi:10.5194/acp-12-3289-2012.
23. Holmes, C.D., Q. Tang, M.J. Prather (2011) Uncertainties in climate assessment: the case of aviation NO_x, *PNAS*, 108(27): 10997-11002, doi: 10.1073/pnas.1101458108.
24. Prather, M.J., X. Zhu, Q. Tang, J. Hsu, J.L. Neu (2011), An atmospheric chemist in search of the tropopause, *J. Geophys. Res.*, 116: D04306, doi:10.1029/2010JD014939.
25. Tang, Qi, M.J. Prather, J. Hsu (2011), Stratosphere-troposphere exchange ozone flux related to deep convection, *Geophys. Res. Lett.*, 38: L03806, doi:10.1029/2010GL046039.
26. PhotoComp (2010), Chapter 6 in SPARC CCMVal Report on Evaluation of Chemistry-Climate Models (V. Eyring, T. G. Shepherd, D. W. Waugh, eds.), SPARC Report No. 5, WCRP-30/2010, WMO/TD – No. 40, www.sparc-climate.org/publications/sparc-reports/.
27. Prather, M.J. and J. Hsu (2010), Coupling of nitrous oxide and methane by global atmospheric chemistry, *Science*, 330: 952-954.
28. Tang, Qi and M.J. Prather (2010), Correlating tropospheric column ozone with tropopause folds: the Aura-OMI satellite data, *Atmos. Chem. Phys.*, 10, 9581-9688.
29. Hsu, Juno and M. J. Prather (2010), Global long-lived chemical modes excited in a 3-D chemistry transport model: Stratospheric N₂O, NO_y, O₃ and CH₄ chemistry, *Geophys. Res. Lett.*, 37, L07805, doi:10.1029/2009GL042243.
30. Prather, M. J. (2009), Tropospheric O₃ from photolysis of O₂, *Geophys. Res. Lett.*, 36, L03811, doi:10.1029/2008GL036851
31. Hsu, J., M. J. Prather (2009), Stratospheric variability and tropospheric ozone, *J. Geophys. Res.*, 114, D06102, doi: 10.1029/2008JD010942
32. Prather M.J., X. Zhu, S.E. Strahan, S.D. Steenrod, J.M. Rodriguez (2008), Quantifying errors in trace species transport modeling, *Proc. Nat. Acad. Sci.* 105(50): 19617-19621.
33. Neu J. L., M. J. Lawler, M. J. Prather, E. S. Saltzman (2008), Oceanic alkyl nitrates as a natural source of tropospheric ozone, *Geophys. Res. Lett.*, 35: L13814.

34. Neu, J.L., M.J. Prather, J.E. Penner (2007) Global atmospheric chemistry: integrating over fractional cloud cover, *J. Geophys. Res.*, 112, D11306.
35. Wild, O. and M.J. Prather (2006) Global tropospheric ozone modeling: Quantifying errors due to grid resolution, *J. Geophys. Res.*, 111(D11), D11305, doi:10.1029/2005JD006605.
36. Hsu, J., M. J. Prather, and O. Wild (2005), Diagnosing the stratosphere-to-troposphere flux of ozone in a chemistry transport model, *J. Geophys. Res.*, 110, D19305, doi:10.1029/2005JD006045.
37. Marandino, C. A., W. J. De Bruyn, S. D. Miller, M. J. Prather, and E. S. Saltzman (2005), Oceanic uptake and the global atmospheric acetone budget, *Geophys. Res. Lett.*, 32, L15806, doi:10.1029/2005GL023285. [see Correction, *GRL* 33(24): Art. No. L24801, 2006.]
38. Ehhalt, D. H., F. Rohrer, S. Schauffler, M. J. Prather (2004) On the decay of stratospheric pollutants: diagnosing the longest-lived eigenmode, *J. Geophys. Res.*, 109(D8), D08102 10.1029/2003JD004029.
39. Wild, Oliver, M. J. Prather, H. Akimoto, J. K. Sundet, I. S. A. Isaksen, J. H. Crawford, D. D. Davis, M. A. Avery, Y. Kondo, G. W. Sachse, S. T. Sandholm (2004) Chemical transport model ozone simulations for spring 2001 over the western Pacific: Regional ozone production and its global impacts, *J. Geophys. Res.*, 109(D15), D15S02, doi:10.1029/2003JD004041.
40. Hsu, Juno, M. J. Prather, O. Wild, J.K. Sundet, I.S.A. Isaksen, E.V. Browell, M.A. Avery, G.W. Sachse (2004) Are the TRACE-P measurements representative of the Western Pacific during March 2001? *J. Geophys. Res.*, 109(D02 314), doi:10.1029/2003JD004002.
41. Wild, O., J.K. Sundet, M.J. Prather, I.S.A. Isaksen, H. Akimoto, E.V. Browell, and S.J. Oltmans (2003) CTM Ozone Simulations for Spring 2001 over the Western Pacific: Comparisons with TRACE-P lidar, ozonesondes and TOMS columns, *J. Geophys. Res.*, 108(D21), 8826, doi:10.1029/2002JD003283.
42. McLinden, C. A., M. J. Prather, M. S. Johnson (2003) Global modeling of the isotopic analogues of N₂O: Stratospheric distributions, budgets, and the 17O–18O mass-independent anomaly, *J. Geophys. Res.*, 108(D8), 4233, doi:10.1029/2002JD002560.
43. Bian, H., M. J. Prather, and T. Takemura (2003) Tropospheric aerosol impacts on trace gas budgets through photolysis, *J. Geophys. Res.*, 108(D8), 4242, doi:10.1029/2002JD002743.
44. Johnston, N. A. C., J. J. Colman, D. R. Blake, M. J. Prather, and F. S. Rowland (2002) On the variability of tropospheric gases: Sampling, loss patterns, and lifetime, *J. Geophys. Res.*, 107(D11), 4111, doi:10.1029/2001JD000669.
45. Bian, H., and M.J. Prather (2002) Fast-J2: Accurate Simulation of stratospheric photolysis in global chemical models, *J. Atmos. Chem.*, 41, 281-296.
46. Gurney K.R., Law R.M., Denning A.S., Rayner P.J., Baker D., Bousquet P., Bruhwiler L., Chen Y.H., Ciais P., Fan S, Fung IY, Gloor M, Heimann M, Higuchi K, John J, Maki T, Maksyutov S, Masarie K, Peylin P, Prather M, Pak BC, Randerson J, Sarmiento J, Taguchi S, Takahashi T, Yuen CW (2002) Towards robust regional estimates of CO₂ sources and sinks using atmospheric transport models, *Nature*, 415, 626-630.
47. Pak, B.C., and M.J. Prather (2001) CO₂ source inversions using satellite observations of the upper troposphere, *Geophys. Res. Lett.*, 28, 4571-4574.
48. Olsen, S. C., C. A. McLinden, and M. J. Prather (2001) The Stratospheric NO_y-N₂O System: Testing uncertainties in a 3-D framework, *J. Geophys. Res.*, 106(D22), 28771-28784.
49. Wild, O., M. J. Prather, H. Akimoto (2001) Indirect long-term global cooling from NO_x emissions, *Geophys. Res. Lett.*, 28, 1719-1722, doi: 10.1029/2000GL012573.
50. Wild, O. and M.J. Prather (2000) Excitation of the primary tropospheric chemical mode in a global three-dimensional model, *J. Geophys. Res.*, 105, 24647-24660.
51. McLinden, C., S. Olsen, B. Hannegan, O. Wild, M. Prather, and J. Sundet (2000) Stratospheric ozone in 3-D models: a simple chemistry and the cross-tropopause flux, *J. Geophys. Res.*, 105, 14653-14665.
52. Wild, O., X. Zhu, and M.J. Prather (2000) Fast-J: Accurate simulation of in- and below-cloud photolysis in tropospheric chemical models, *J. Atmos. Chem.*, 37, 245-282.
53. Olsen, S.C., B. J. Hannegan, X. Zhu, and M.J. Prather (2000) Evaluating ozone depletion from very short-lived halocarbons, *Geophys. Res. Lett.*, 27, 1475-1478.
54. Hall, T.M., D.W. Waugh, K.A. Boering, R.A. Plumb (1999) Evaluation of transport in stratospheric models, *J. Geophys. Res.* 104, 18815-18139, doi: 10.1029/1999JD900226.

55. Hannegan, B. S. Olsen, M. Prather, X. Zhu, D. Rind, and J. Lerner (1998) The dry stratosphere: A limit on cometary water influx, *Geophys. Res. Lett.*, 25, 1649-1652.
56. Ehhalt, D.H., F. Rohrer, A. Wahner, M.J. Prather, and D.R. Blake (1998) On the use of hydrocarbons for the determination of tropospheric OH concentrations, *J. Geophys. Res.* 103, 18981-18997.
57. Avallone, L.M. and M.J. Prather (1997) Tracer-tracer correlations: three-dimensional model simulations and comparisons to observations, *J. Geophys. Res.*, 102, 19233-19246.
58. Ehhalt, D.H., F. Rohrer, A.B. Kraus, M.J. Prather, D.R. Blake, and F.S. Rowland (1997) On the significance of regional trace gas distributions as derived from aircraft campaigns in PEM-West A and B, *J. Geophys. Res.* 102, 28333-28351.
59. Hall, T.M. & M.J. Prather (1995) Seasonal evolution of N₂O, O₃, and CO₂: three-dimensional simulations of stratospheric correlations, *J. Geophys. Res.*, 100, 16699-16720.
60. Hall, T.M., & M.J. Prather (1993) Simulations of the Trend and Annual Cycle in Stratospheric CO₂, *J. Geophys. Res.*, 98, 10573-10581.
61. Fung, I., J. John, J. Lerner, E. Matthews, M. Prather, L.P. Steele and P.J. Fraser (1991) Three-Dimensional Model Synthesis of the Global Methane Cycle, *J. Geophys. Res.*, 96, 13,033-13,065.
62. Jacob, D.J. and M.J. Prather (1990) Radon-222 as a test of the boundary-layer convection in a general circulation model, *Tellus* 42B, 118-134.
63. Prather, M., M.M. Garcia, R. Suozzo and D. Rind (1990) Global impact of the Antarctic ozone hole: dynamical dilution with a 3-D chemical transport model, *J. Geophys. Res.* 95, 3449-3471.
64. Prather, M.J. & J.M. Rodriguez (1988) Antarctic ozone: meteoric control of HNO₃, *Geophys. Res. Lett.* 15, 1-4, doi: 10.1029/GL015i001p00001.
65. Prather, M., M. McElroy, S. Wofsy, G. Russell and D. Rind (1987) Chemistry of the global troposphere: fluorocarbons as tracers of air motion, *J. Geophys. Res.* 92, 6579-6613.
66. Prather, M.J. (1986) Numerical advection by conservation of second-order moments. *J. Geophys. Res.* 91, 6671-6681, doi: 10.1029/JD091iD06p06671

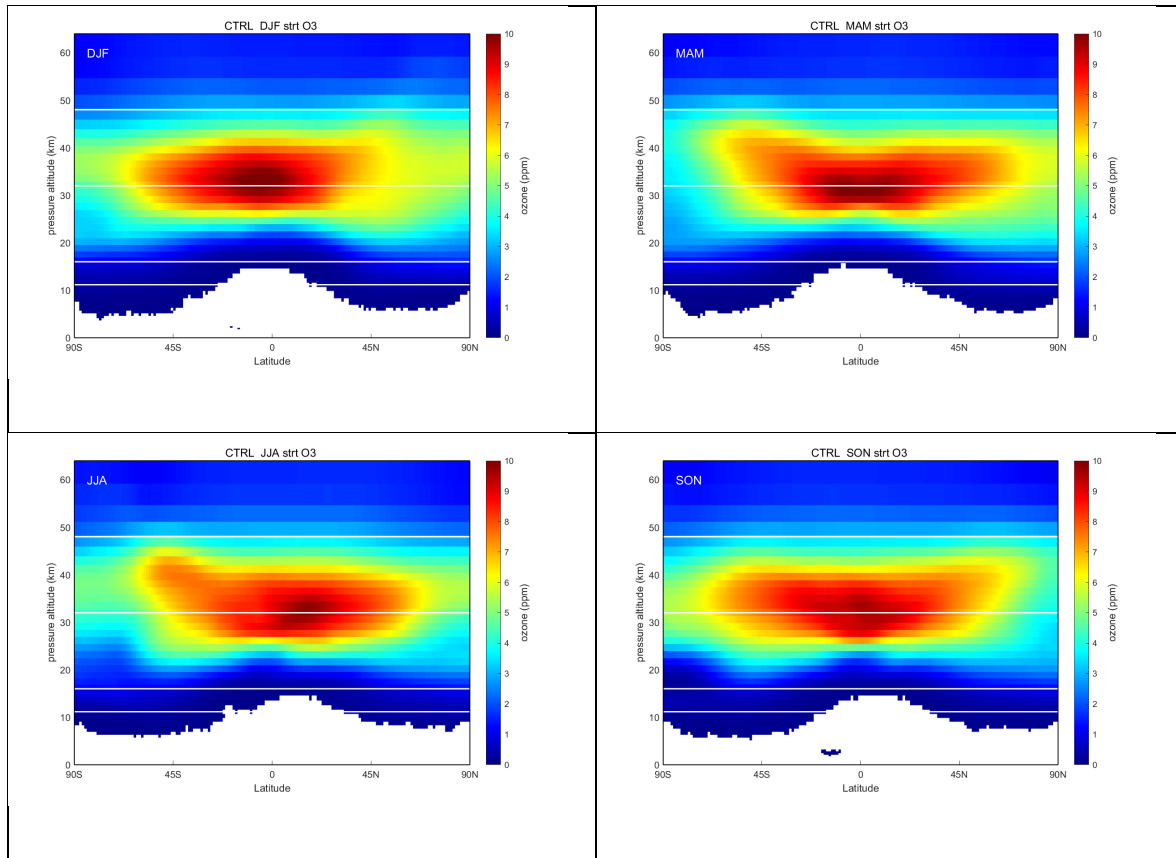


Figure A1. Stratospheric zonal mean O₃ abundance (ppm) averaged over four seasons (DJF, MAM, JJA, SON) comprised of 5-day snapshots from year 2003 of the CTRL run. Coordinates are latitude by pressure altitude $z^* = 16 \text{ km} \log_{10}(1/P(\text{bars}))$ and assume a surface pressure everywhere of 1 bar.

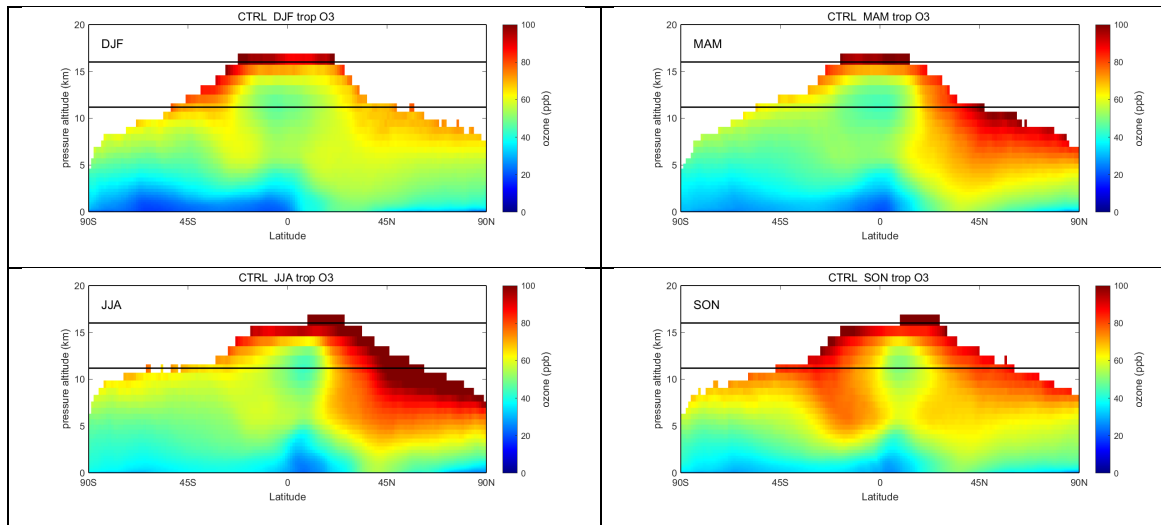


Figure A2. Tropospheric zonal mean O₃ abundance (ppb), see Fig. A1. Some pixels in Fig. A1 and A2 contain both stratospheric and tropospheric values because the pixel contained was both stratospheric and tropospheric air over the 18 snapshots and 320 longitude cells (e.g., stratospheric intrusions).

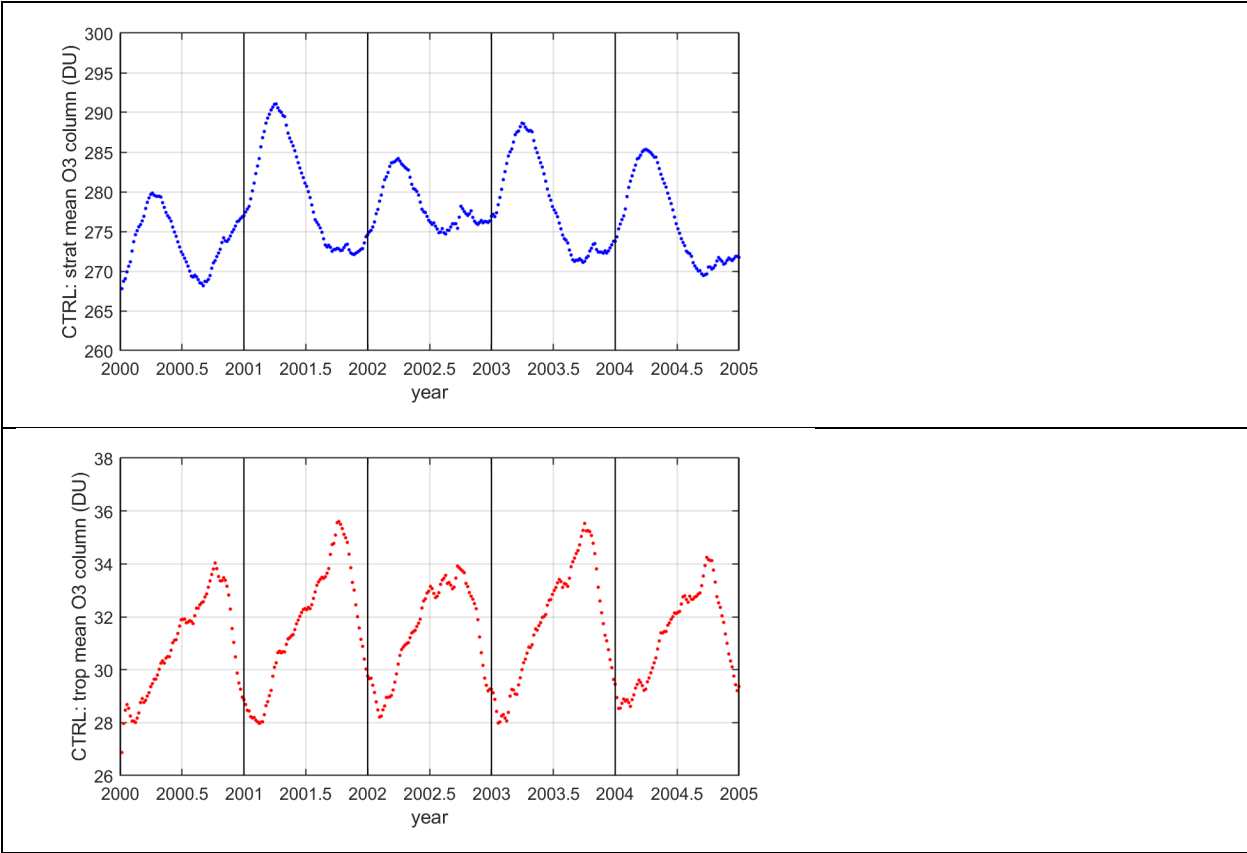


Figure A3. Stratospheric (top) and tropospheric (bottom) global mean O₃ columns (DU) from the CTRL run calculated from the 365 5-day snapshots over the five years, 2000 through 2004.

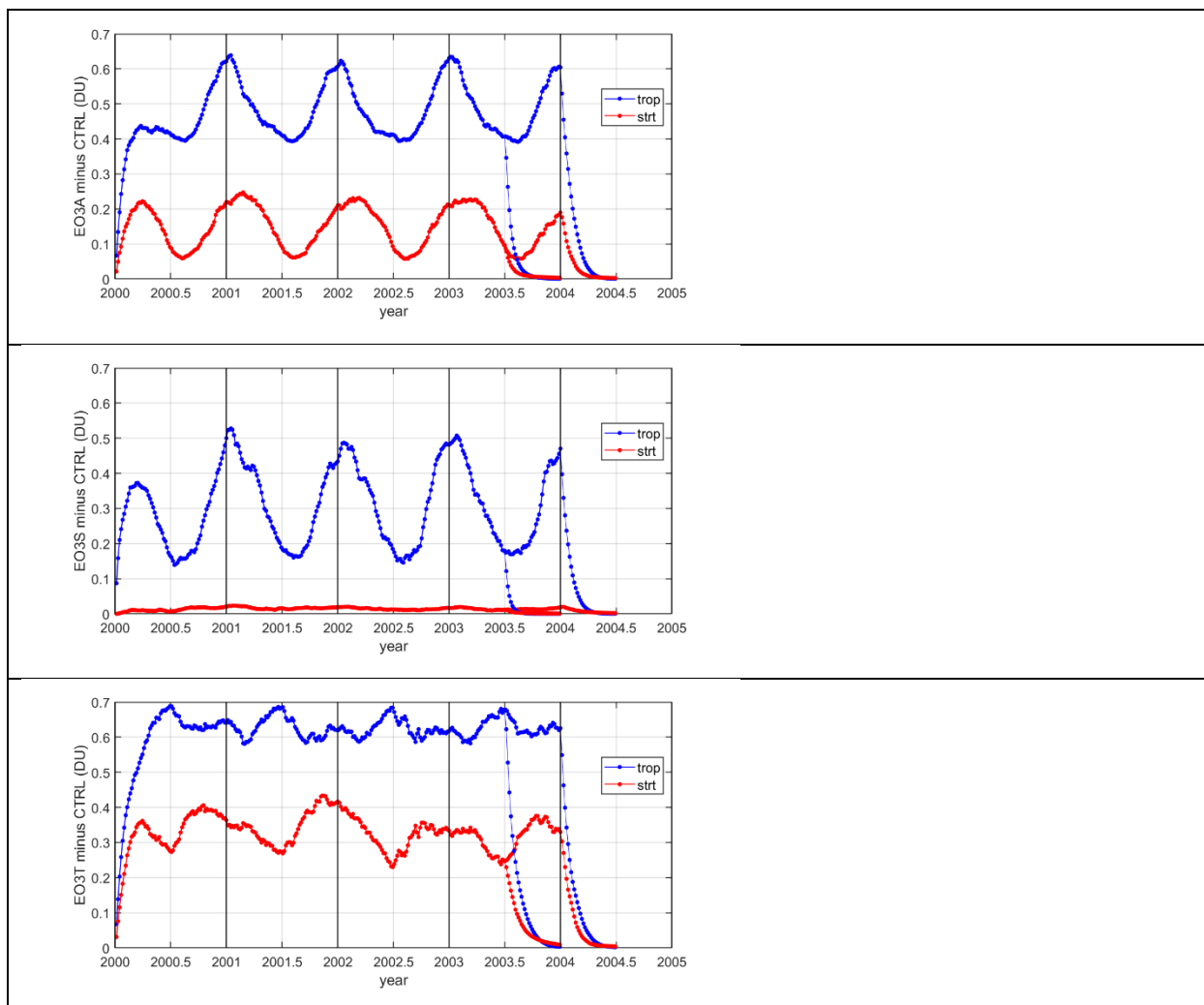


Figure A4. Perturbation in the O₃ column (DU) for eO3avi (EO3A, top), eO3srf (EO3S, middle), and eO3stel (EO3T, bottom), separating troposphere (blue) from stratosphere (red). Also shown are the decay of the perturbations following cessation of emissions on July 1 (2003.5) and Jan 1 (2004.0). In terms of DU, the annual emissions are about 9.2 DU, and thus a tropospheric perturbation of 0.4 DU has a lifetime of 16 days.

eO3avi (EO3A)

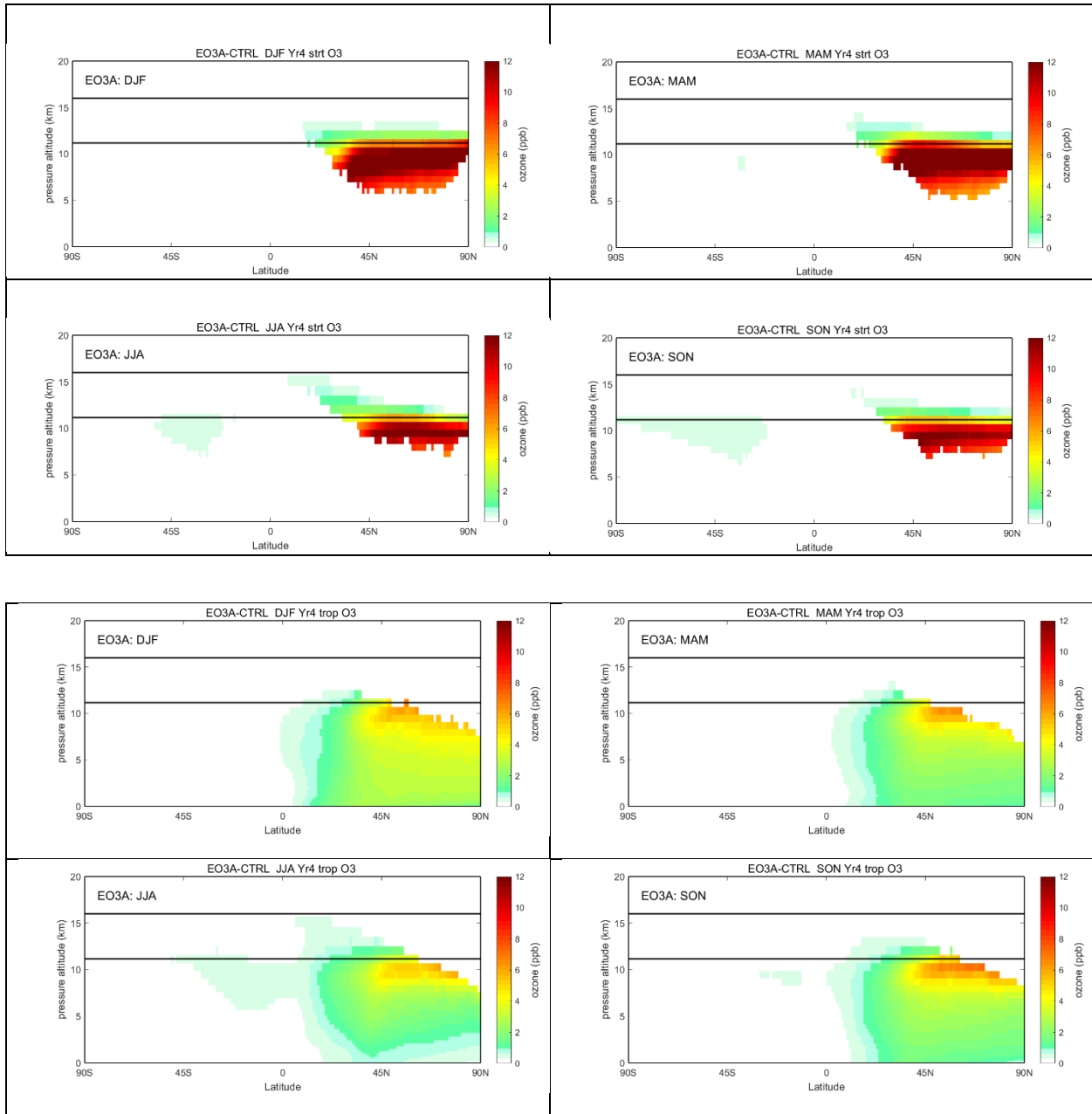


Figure A5. eO3avi perturbation to zonal mean O₃ abundance (ppb) for four seasons (DJF, MAM, JJA, SON), split into stratospheric (top panels) and tropospheric (bottom panels). For methodology, see Figure A1. Aviation emissions (eO3avi) occur mostly in the northern troposphere but reach into the stratosphere and southern hemisphere. Note that color bars have the same range on all plots.

eNOavi (EO3B)

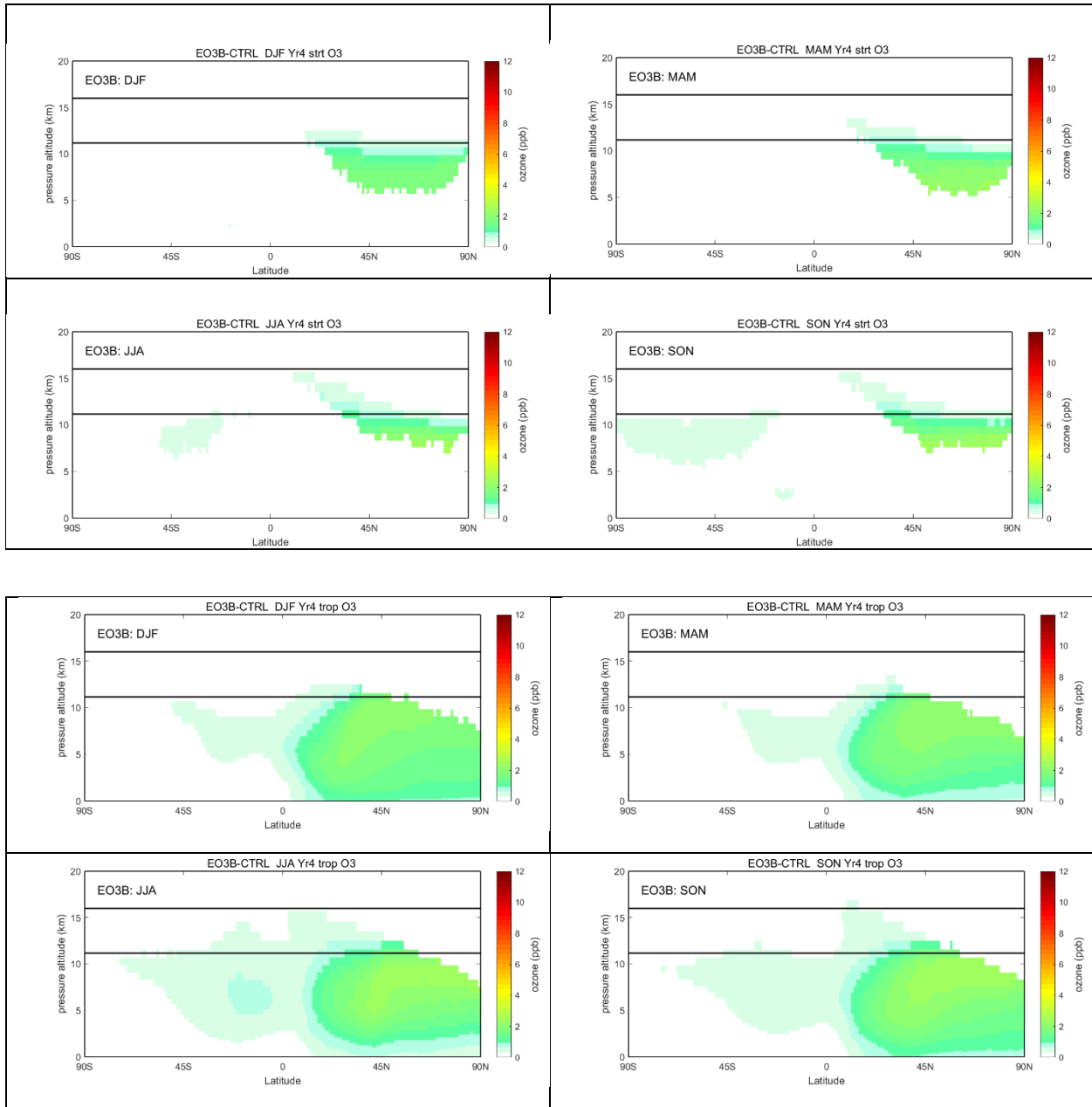


Figure A6. eNOavi perturbation to zonal mean O₃ abundance (ppb) for four seasons (DJF, MAM, JJA, SON), split into stratospheric (top panels) and tropospheric (bottom panels). For methodology, see Figure A1. Aviation emissions (eNOavi) occur as NO_x. Note that color bars have the same range on all plots.

eO3srf (EO3S)

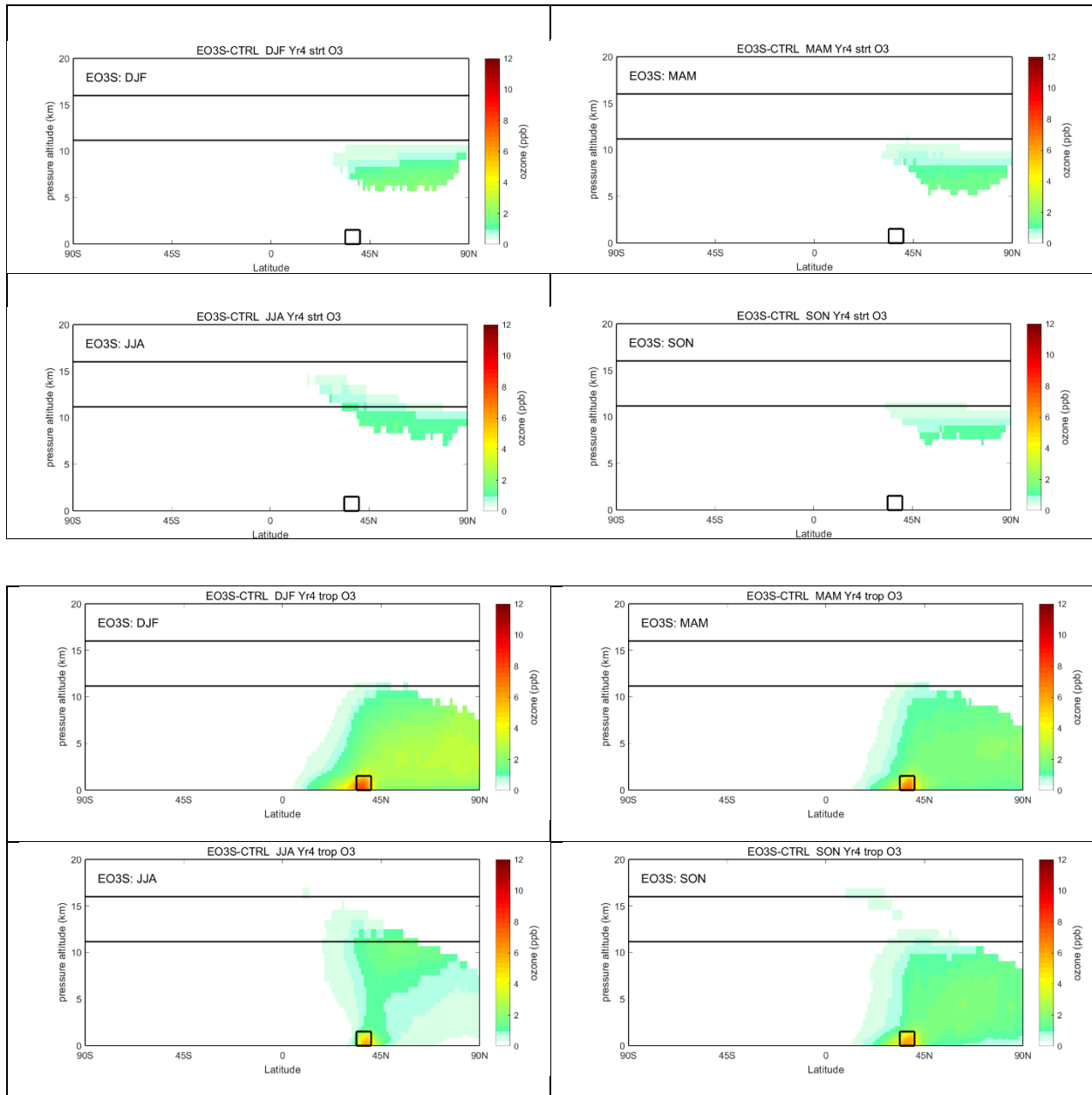


Figure A7. eO₃srf perturbation to zonal mean O₃ abundance (ppb) for four seasons (DJF, MAM, JJA, SON), split into stratospheric (top panels) and tropospheric (bottom panels). For methodology, see Figure A1. Surface emissions (eO₃srf) occur within the black square over a limited longitude range, see Table 1.

eO3ste1 (EO3T)

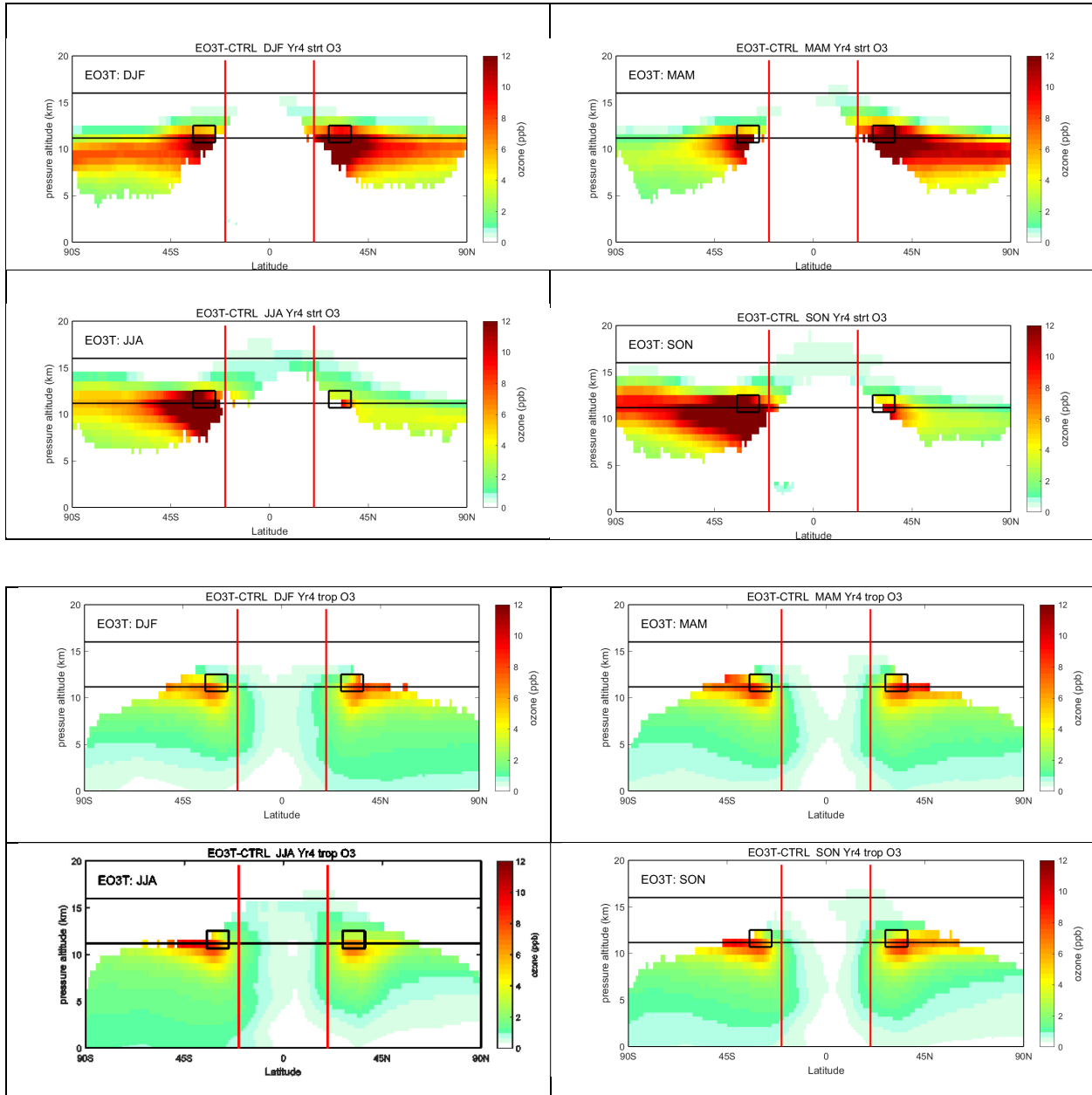


Figure A8. eO3ste1 perturbation to zonal mean O₃ abundance (ppb) for four seasons (DJF, MAM, JJA, SON), split into stratospheric (top panels) and tropospheric (bottom panels). For methodology, see Figure A1. STE emissions (eO3ste1) occur within the black squares equally in each hemisphere and across all longitudes, see Table 1.

eO3ste2 (EO3U)

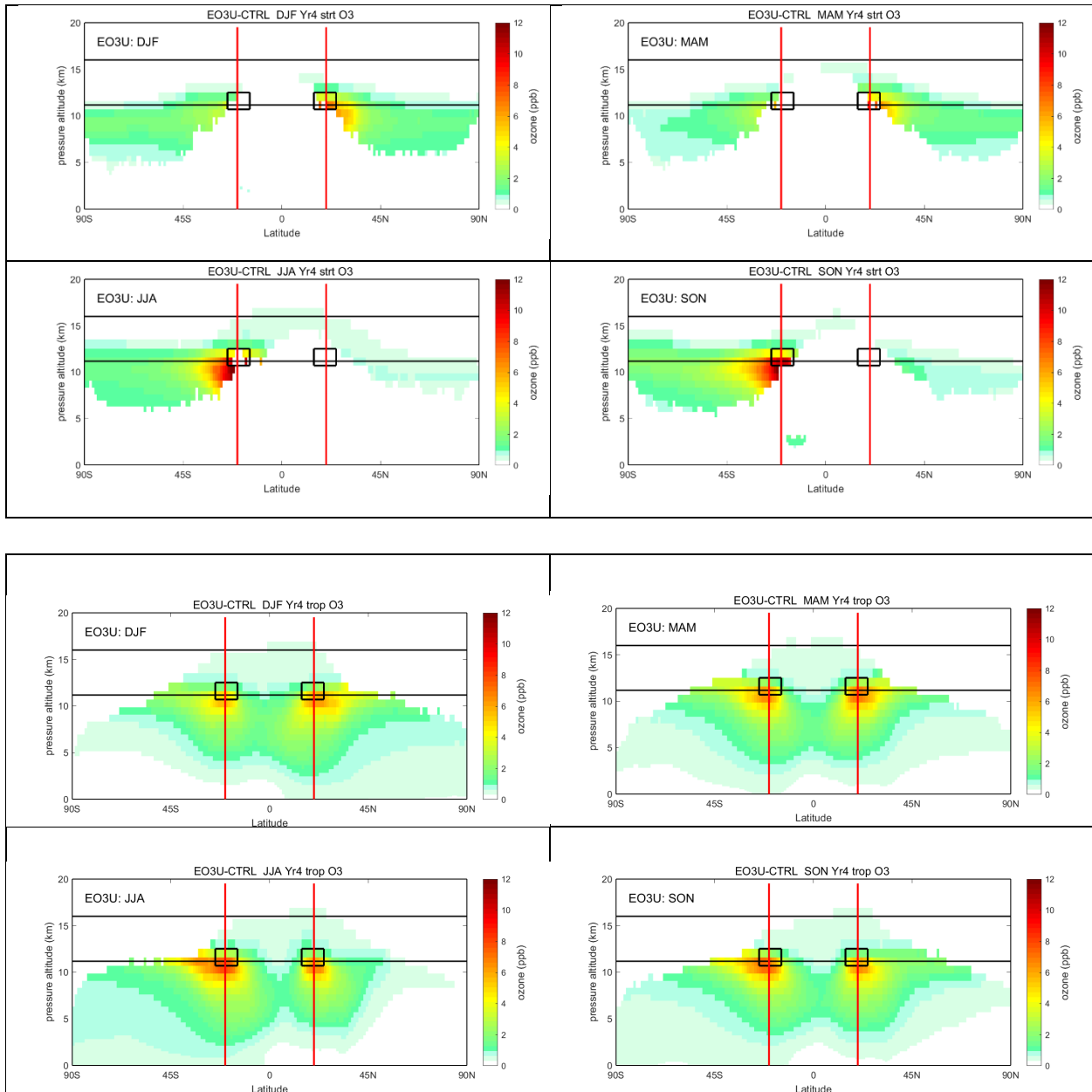


Figure A9. eO3ste2 perturbation to zonal mean O₃ abundance (ppb) for four seasons (DJF, MAM, JJA, SON), split into stratospheric (top panels) and tropospheric (bottom panels). For methodology, see Figure A1. STE emissions (eO3ste2) occur within the black squares equally in each hemisphere and across all longitudes, see Table 1.

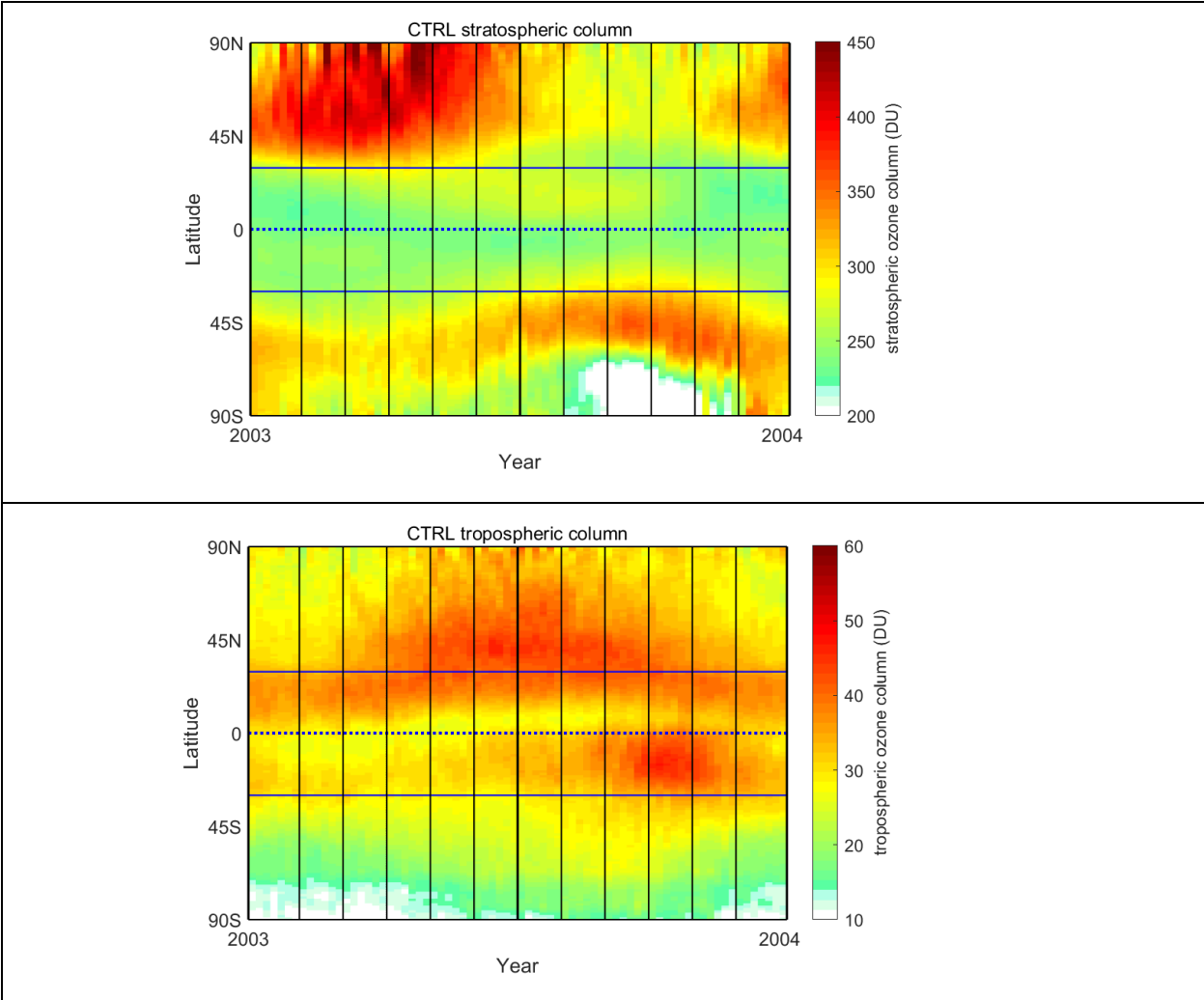


Figure A10. Stratospheric (top) and tropospheric (bottom) O₃ column (DU) for year 2003 from the control (CTRL) simulation. Columns are a function of latitude and time at 5-day intervals.

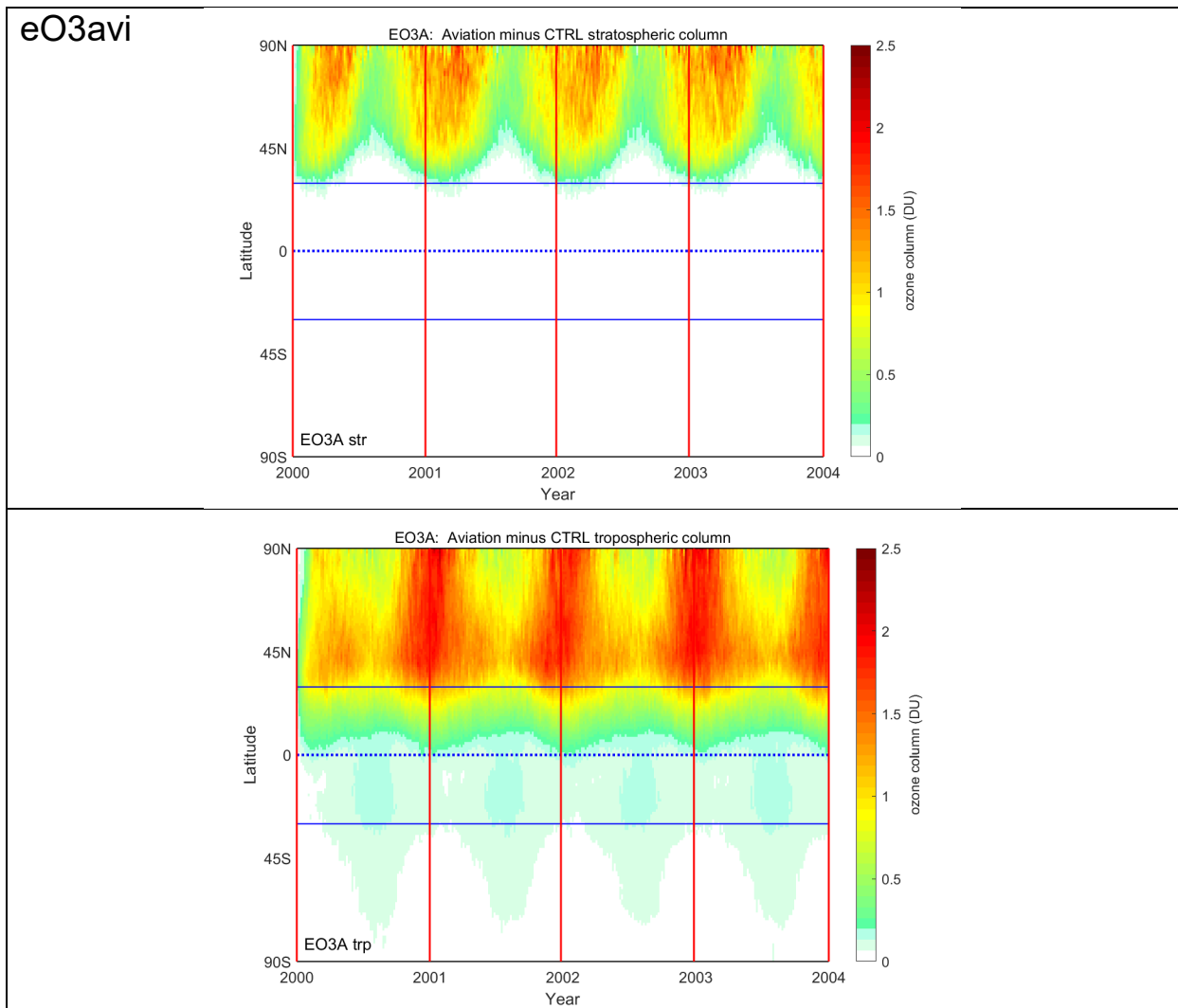


Figure A11. Ozone column perturbation (DU) for experiment eO3avi (aviation O₃) as a function of latitude and time (2000.0 to 2004.0) at 5-day intervals for stratosphere (top) and troposphere (bottom).

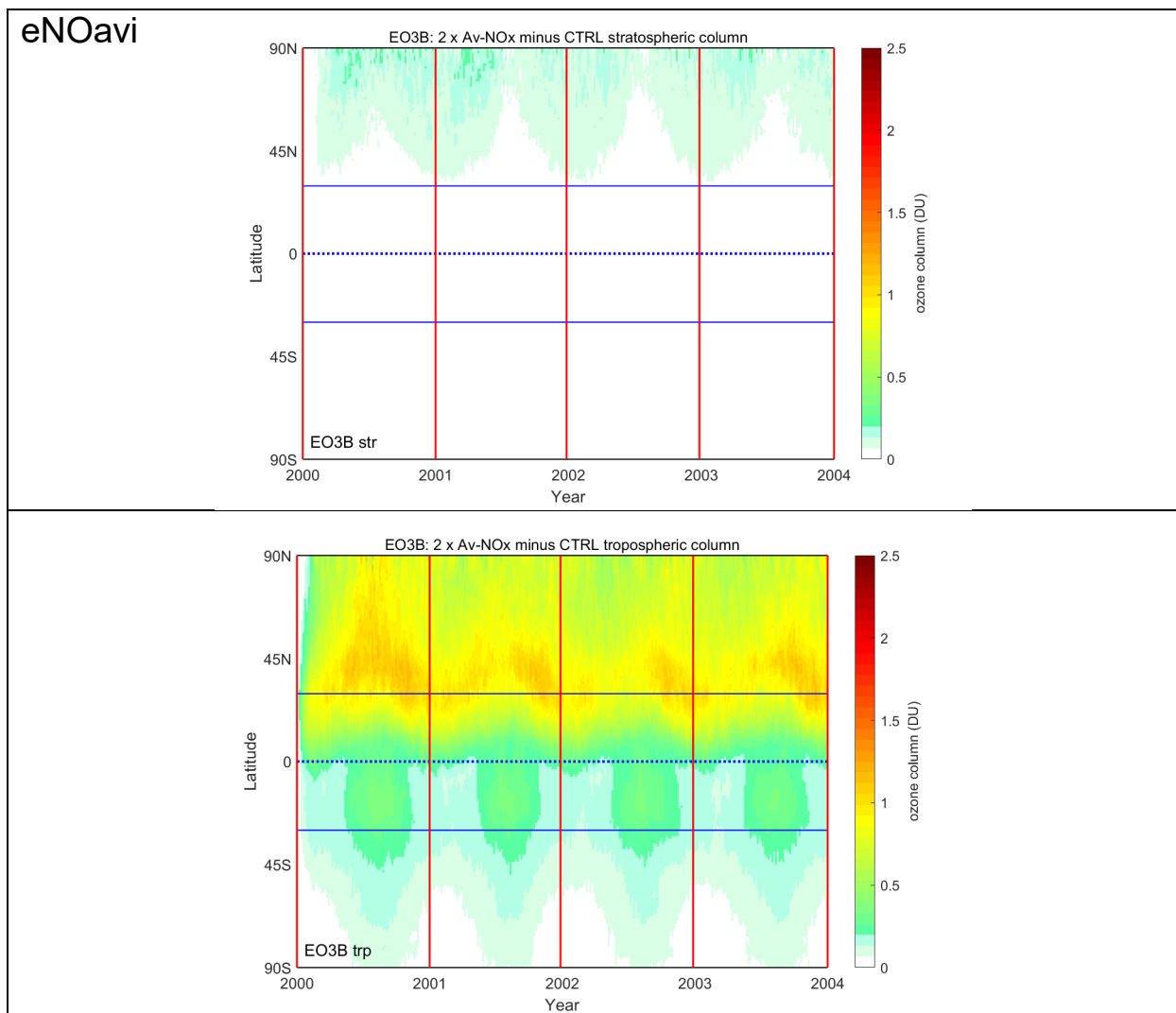


Figure A12. Ozone column perturbation (DU) for experiment eNOavi (aviation NO_x) as a function of latitude and time (2000.0 to 2004.0) at 5-day intervals for stratosphere (top) and troposphere (bottom).

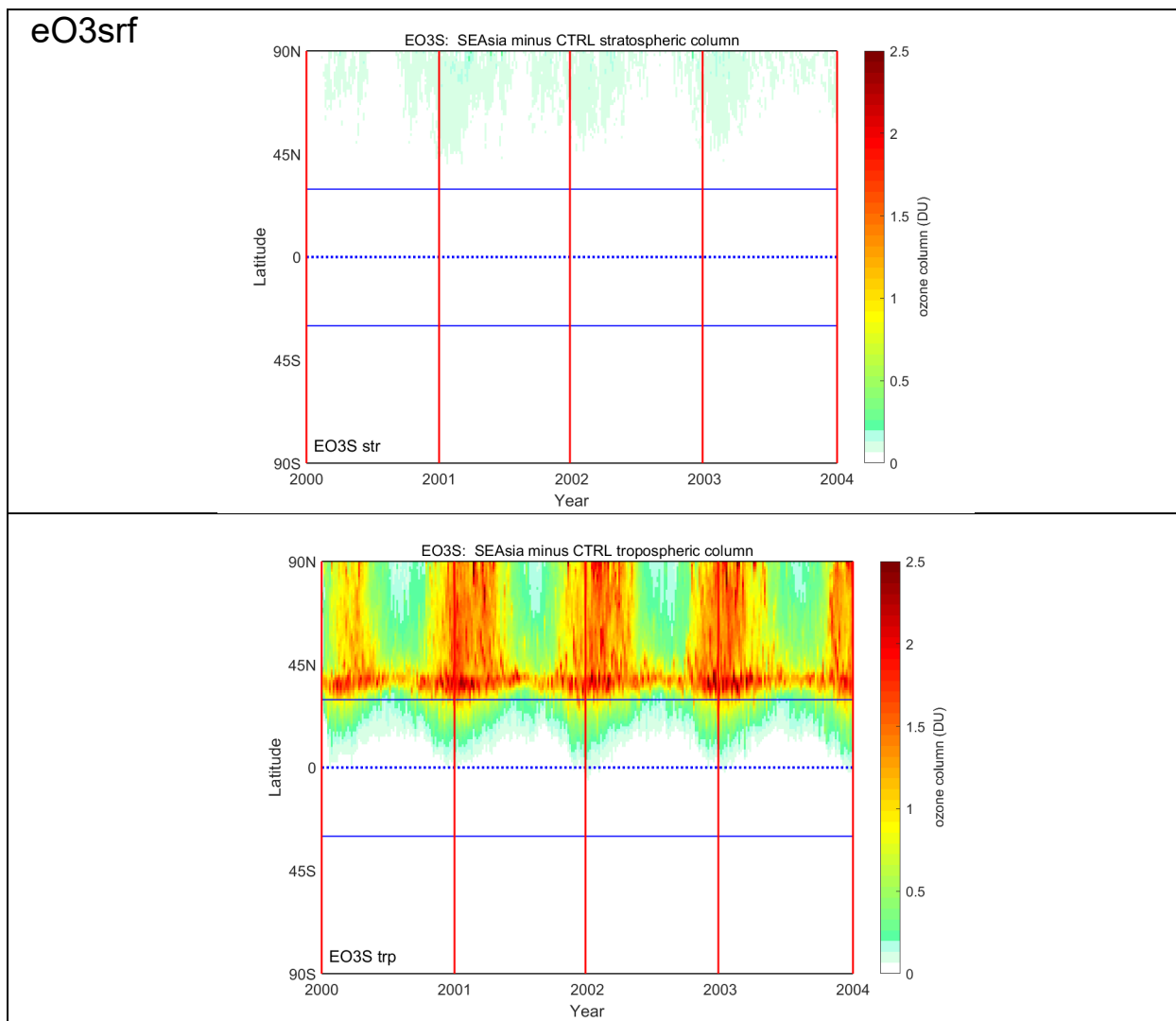


Figure A13. Ozone column perturbation (DU) for experiment eO3srf (surface O₃) as a function of latitude and time (2000.0 to 2004.0) at 5-day intervals for stratosphere (top) and troposphere (bottom).

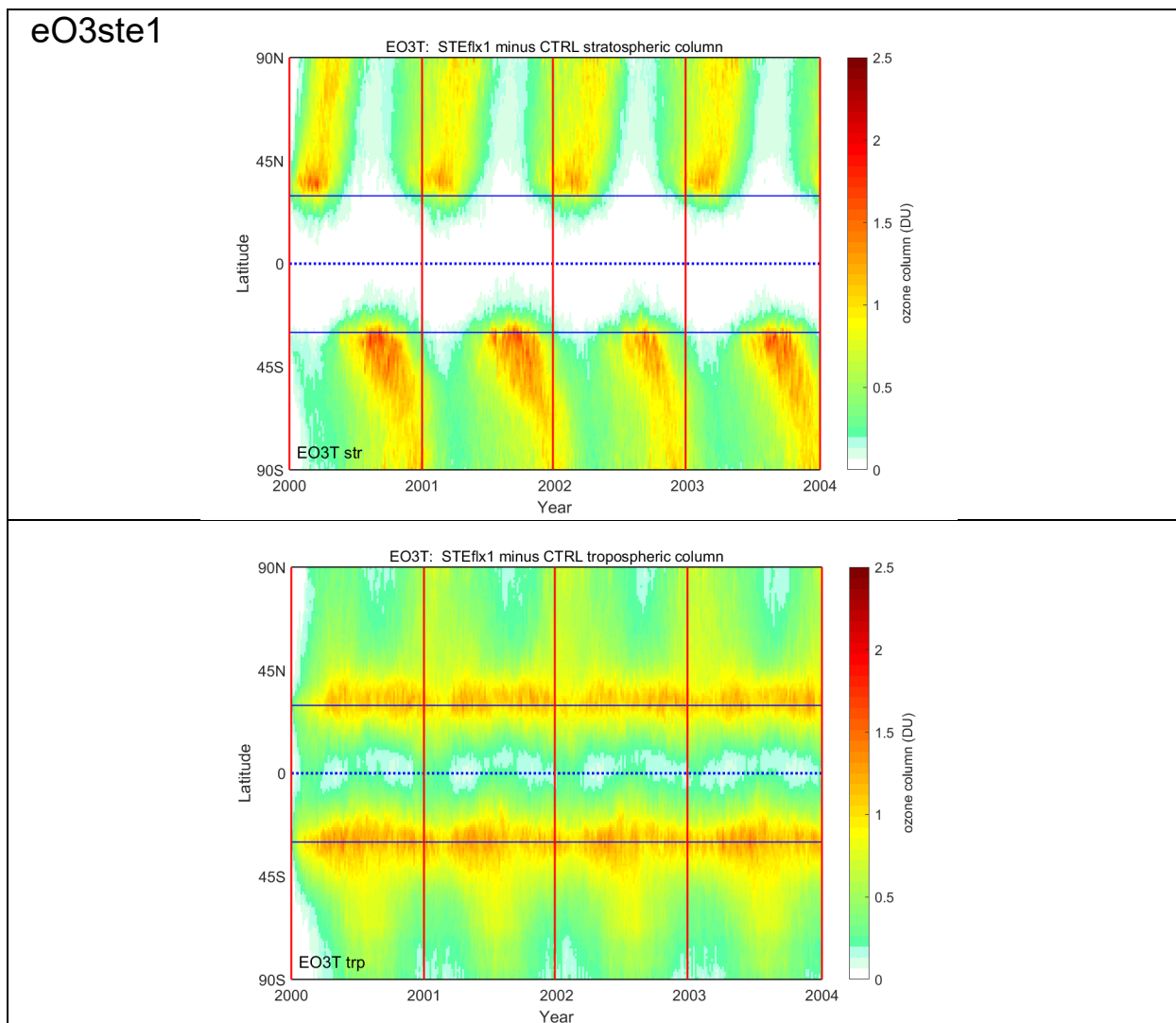


Figure A14. Ozone column perturbation (DU) for experiment eO3ste1 (1st STE O₃) as a function of latitude and time (2000.0 to 2004.0) at 5-day intervals for stratosphere (top) and troposphere (bottom).

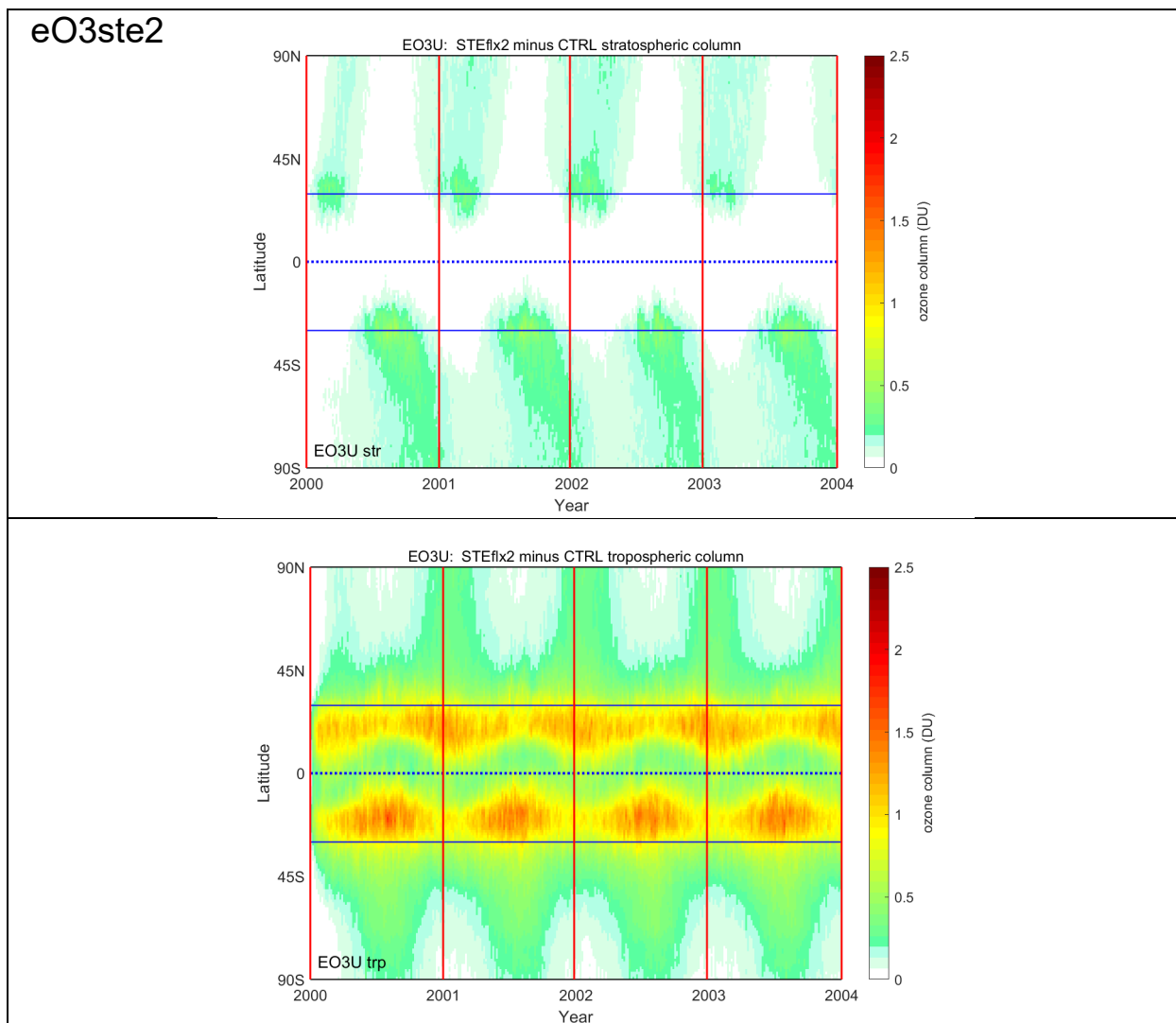


Figure A15. Ozone column perturbation (DU) for experiment eO3ste2 (2nd STE O₃) as a function of latitude and time (2000.0 to 2004.0) at 5-day intervals for stratosphere (top) and troposphere (bottom).

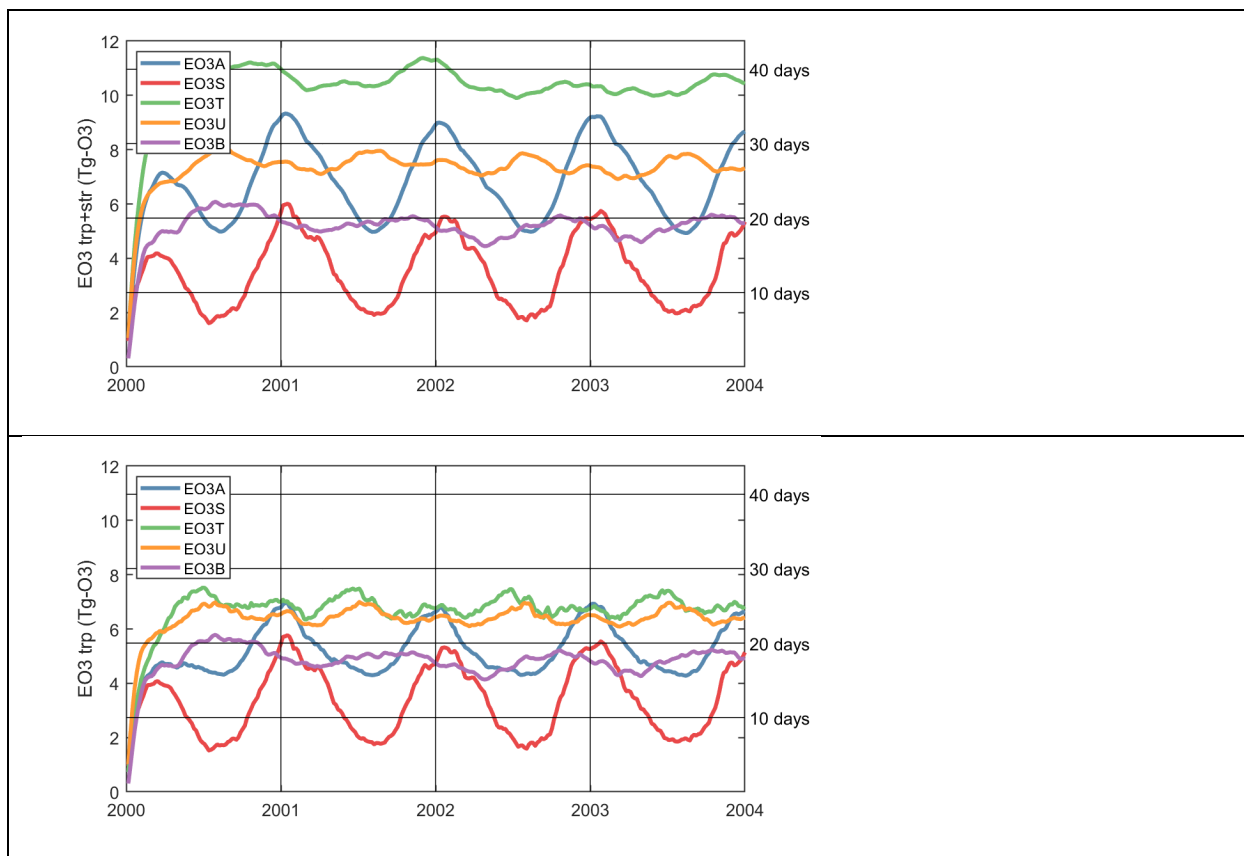


Figure A16. Total (top) and tropospheric (bottom) burden of excess O₃ (Tg) for the five experiments, showing 5-day intervals for years 2000 through 2003. The spin up in early 2000 is clearly visible. The lifetime scale (days, right axis) is calculated from the emission rate of 100 Tg-O₃ yr⁻¹ for both tropospheric and total burden, and it does not apply to eNO_{avi}. The legend notation is: EO3A = eO3_{avi}; EO3S = eO3_{srf}; EO3T = eO3_{ste1}; EO3U = eO3_{ste2}; EO3B = eNO_{avi}..

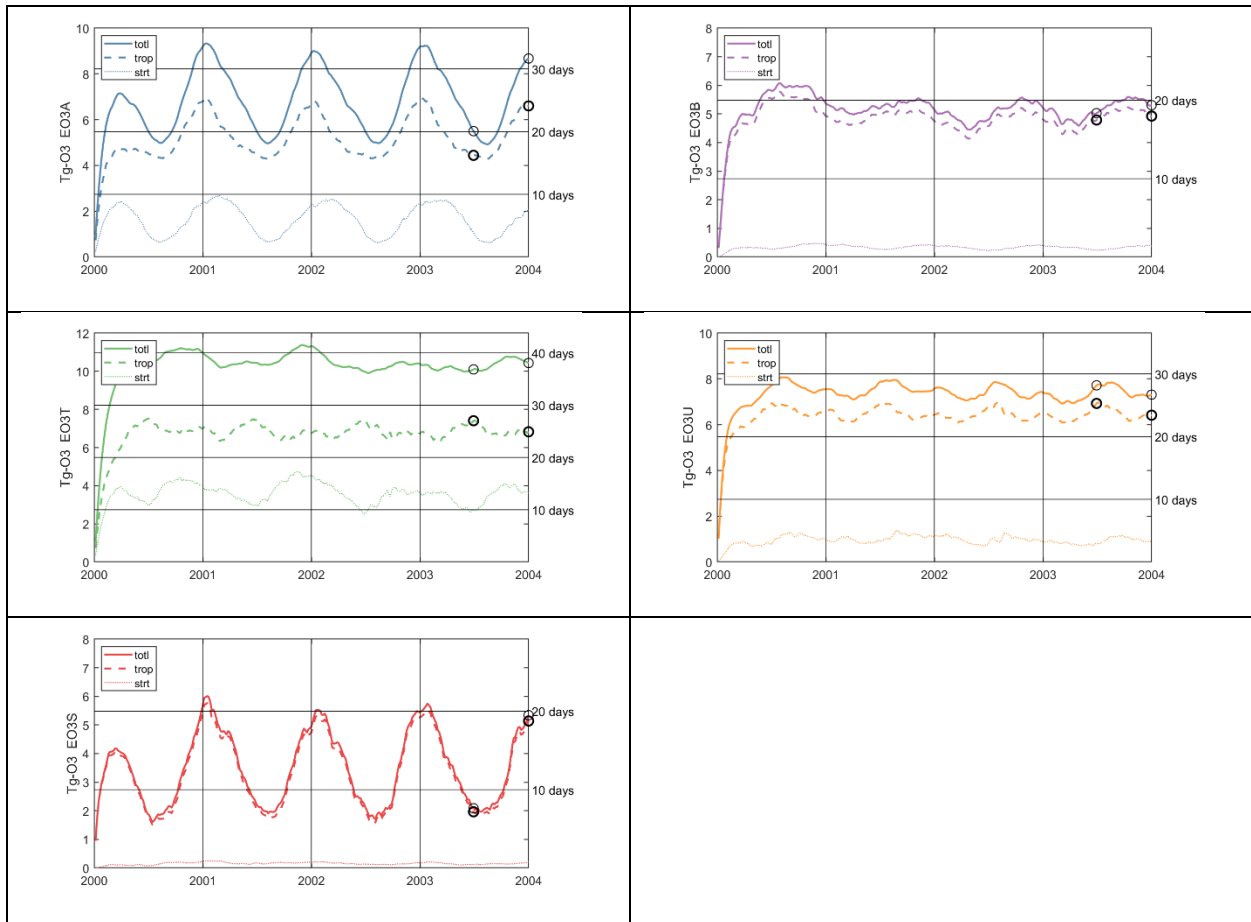


Figure A17. Burden of excess O₃ (Tg) for the five experiments. For each experiment, the tropospheric (dashed line), stratospheric (dotted line) and total (solid line) are shown. See Figure A16. The y-axis notation is: EO3A = eO3avi; EO3S = eO3srf; EO3T = eO3ste1; EO3U = eO3ste2; EO3B = eNOavi;

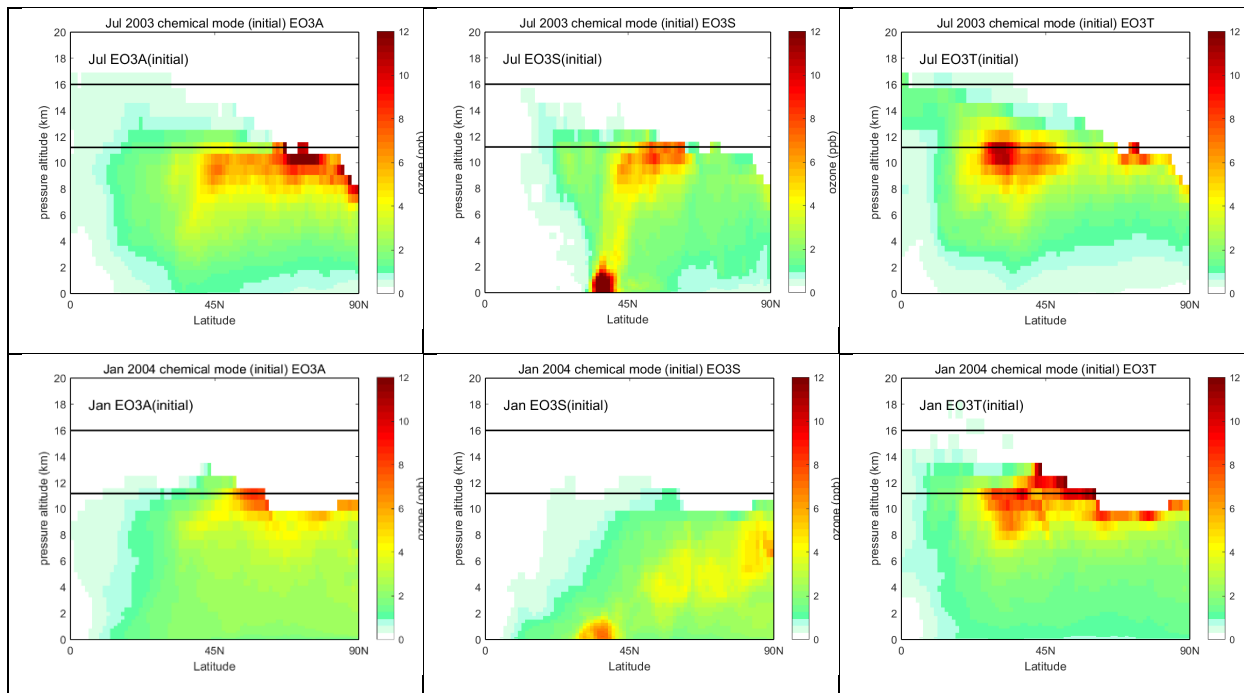


Figure 18. Instantaneous patterns of NH tropospheric O_3 perturbation for eO3avi/srf/stel1 at 1 Jul 2003 and 1 Jan 2004. All patterns are scaled to a total of 5 Tg. Figure titles: EO3A = eO3avi; EO3S = eO3srf; EO3T = eO3stel.

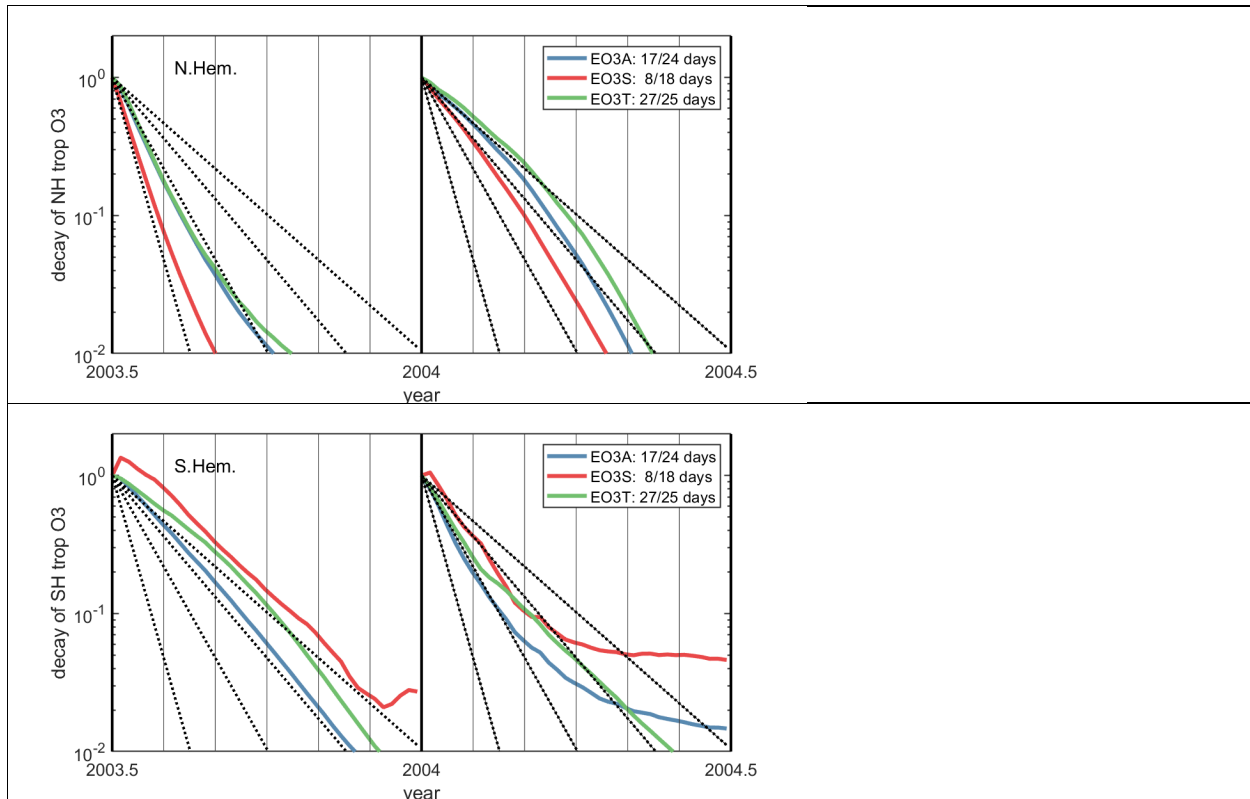


Figure A19. (top) Decay of northern hemisphere tropospheric O₃ perturbations (Tg) for eO3avi/srf/ste1 rescaled to 1 at the time of cessation of emissions on July 1 (left) and January 1 (right). Dashed black lines are the same in both panels and show a constant decay of 10- (steepest), 20-, 30- and 40-day e-folds. The legend gives the min-to-max range in steady-state lifetime. Months are marked with vertical lines. (bottom) Same plot for southern hemisphere tropospheric O₃. The legend notation is: EO3A = eO3avi; EO3S = eO3srf; EO3T = eO3ste1.

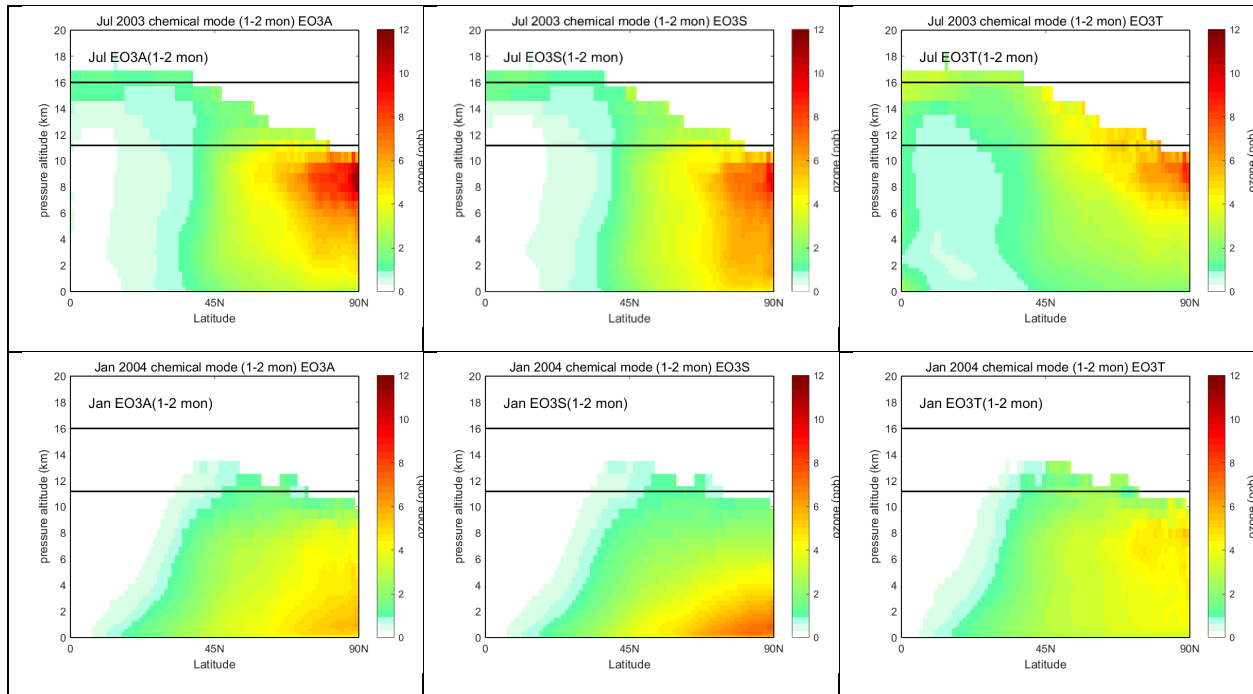


Figure A20. Chemical mode patterns for the troposphere following decay of eO3avi/srf/stel1 starting at 1 Jul 2003 and 1 Jan 2004. Modes are calculated from averaged NH patterns after 1-2 months decay (days 30-85). All perturbations are scaled to a total NH tropospheric O₃ perturbation of 5 Tg.

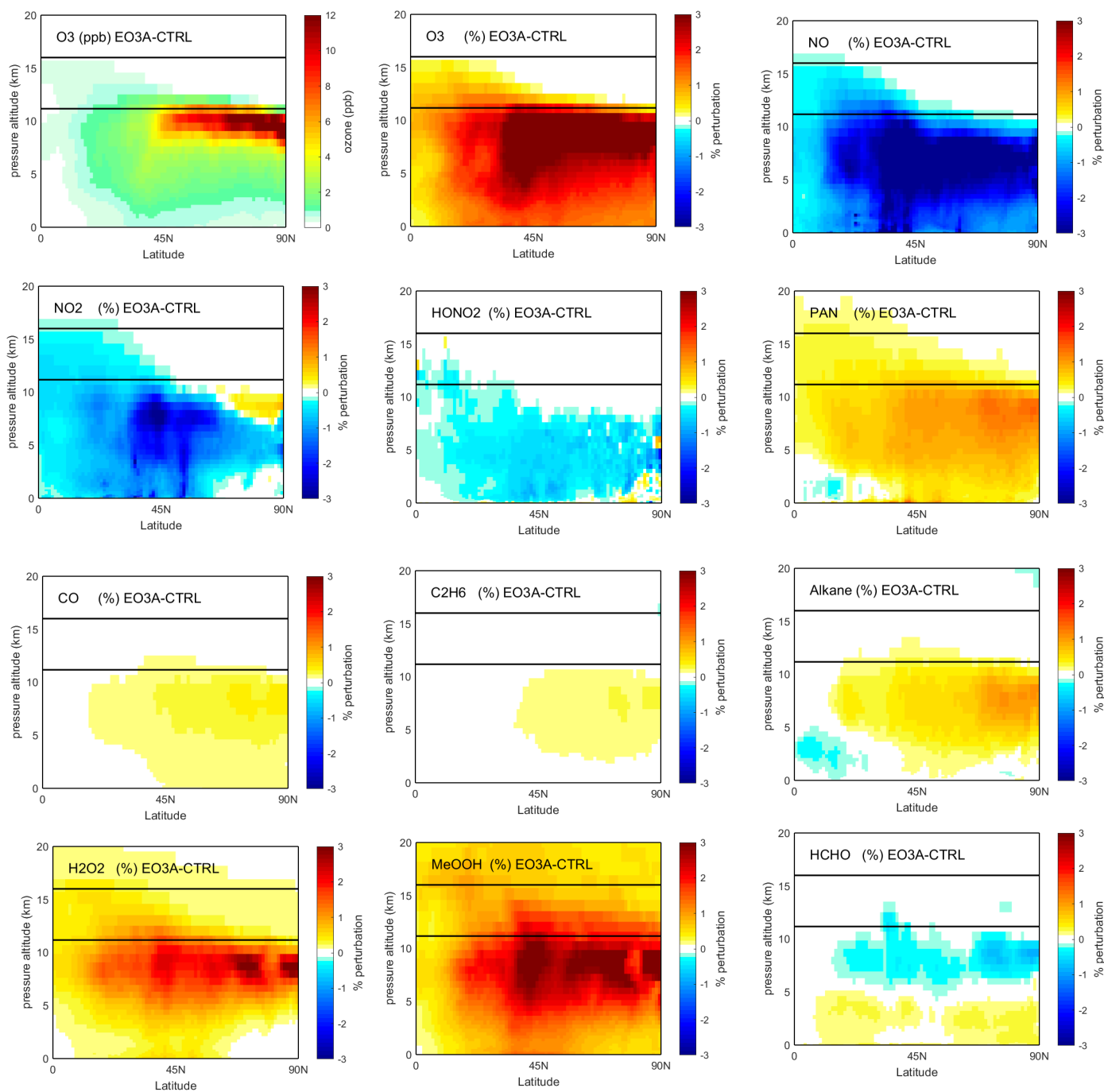


Figure A21. Latitude-by-altitude plots of the perturbations to key chemical species for the eO3avi (aviation) vs. CTRL on 1 Jul 2003. The upper-left-corner panel shows the O₃ perturbation in ppb to compare with earlier figures. All other panels, including the 2nd O₃ panel are in % difference. Note that the color bar, -3% to +3%, is the same for the eleven relative change panels.